Document Number
TRACOR 66-136-U

TECHNICAL MEMORANDUM

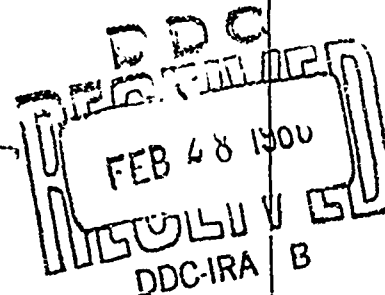A PARAMETRIC ANALYSIS OF DOME-TRANSDUCER INTERACTIONS

Prepared for the

Chief, Bureau of Ships
Department of the Navy
Washington, D. C.

Attention: Code 1622E

Contract NObsr-91229
Project Serial Number SF101-03-17
Task 8139

February 10, 1966

TRACOR
INC.

TRACOR, INC.   6500 TRACOR LANE, AUSTIN, TEXAS 78721

Document Number
TRACOR 66-136-U

TECHNICAL MEMORANDUM

A PARAMETRIC ANALYSIS OF DOME-TRANSDUCER INTERACTIONS

Prepared for the

Chief, Bureau of Ships
Department of the Navy
Washington, D. C.

Attention: Code 1622E

Contract NObsr-91229
Project Serial Number SF101-03-17
Task 8139

February 10, 1966

Prepared by:

W. C. Moyer
W. C. Moyer

J. D. Morell
J. D. Morell

Document Number
TRACOR 66-136-U

TRACOR, INC.   6500 TRACOR LANE, AUSTIN, TEXAS 78721

ABSTRACT

This technical memorandum presents some results of a parametric analysis of the interaction of sonar domes and transducers during transmission. The results were obtained from the numerical evaluation of an analytical model consisting of a cylindrical transducer and concentric dome. The dome-transducer parameters considered in this study include dome-transducer spacing, transducer diameter, transmitting frequency, dome thickness, and material properties of the dome. The parameter ranges include values appropriate to the AN/SQS-4, AN/SQS-23, and AN/SQS-26 systems. The results are presented as functions of the dimensionless products of the dome-transducer parameters. In this form, the results represent an initial effort at formulating guidelines which have broad application in dome design. Improved guidelines will be generated as better analytical models of the dome-transducer are developed.

The results show that the dome produces a degradation of each of the performance criteria compared to a bare transducer. The effects of the dome can be reduced, however, by proper choice of dome parameters. The results provide a quantitative measure of the relative importance of the various parameters in determining degradation in performance due to the dome. It is shown that the product of dome material density and thickness (surface density) is the most important parameter in determining the effect of the dome on transducer performance.

TRACOR, INC.   6500 TRACOR LANE, AUSTIN, TEXAS 78721

TABLE OF CONTENTS

LIST OF FIGURES

LIST OF FIGURES (Cont'd)

I.   INTRODUCTION

A set of design goals or performance criteria and an
analytical model of the dome-transducer are two of the ingredi-
ents necessary in the development of guidelines for dome design.
Guidelines are generated by determining the functional dependence
of each of the performance criteria on the parameters of the dome-
transducer system. By choosing those parameter values which
optimize the performance criteria, the designer is led, hopefully,
to an optimum dome design. The current inadequacy of design
information is due basically to inadequate models for dome-
transducer interactions.

This technical memorandum presents the results of an
initial effort to generate dome design guidelines. While the
dome-transducer model is not yet completely realistic in terms
of dome geometry, the type of information and method of presenta-
tion of the results should be representative of design guideline
requirements. The guidelines presented herein were generated by
computing the dependence of certain performance criteria on the
parameters of a dome-transducer model consisting of a cylindrical
transducer and concentric dome.[1] The performance criteria
considered in this study include:

1. Directivity Index

2. Major Lobe Width

3. Side Lobe Level

4. Dome Transmission Coefficient

5. Dome Transfer Coefficient

6. Nearfield Roughness.

The first three quantities are familiar measures of the farfield
characteristics of a dome-transducer.

Dome Transmission Coefficient is a measure of the per-
centage of energy incident on the dome which is transmitted to

1

the farfield. A portion of the incident energy is reflected within the dome and is not transmitted to the farfield. These reflections form standing waves between the dome and transducer and affect the coupling of the transducer to the medium.

Dome Transfer Coefficient is a measure of the coupling between transducer and dome and is a function of system geometry. Proper coupling results in an efficient power transfer from the transducer to the medium.

Nearfield Roughness is related to the transducer source level. In a typical transducer, element mutual interactions and dome-transducer interactions produce "roughness" or non-uniformity in the nearfield sound pressure distribution. It is desirable to maintain a smooth nearfield pressure distribution; otherwise, it may be necessary to reduce the transducer source level in order to keep the nearfield sound pressure peaks below the cavitation limit. Consequently, nearfield roughness can be an important performance criterion consistent with obtaining maximum source level.

The computed results for performance criteria are presented as functions of dimensionless products of the dome-transducer parameters. This method of presentation does not limit the results to a specific sonar system but enables the results to be applied to any system whose configuration is compatible with the parameter ranges used in the computations. The parameter ranges include values appropriate to the AN/SQS-4, AN/SQS-23, and AN/SQS-26 systems.

In addition to the specific results, some general conclusions concerning the effects of domes on sonar performance are included. A summary of the results and their implications in dome design are given also.

2

II.   ANALYSIS

This section contains a brief discussion of the dome-transducer model used for the analysis described in this memorandum, the definitions of the performance criteria, and the formulation of a method of presentation of the results.

A. Dome-Transducer Model

The dome-transducer model consists of a cylindrical transducer of radius "a" surrounded by a homogeneous, elastic shell of radius "b" and thickness "h." (See Fig. 1.) The problem, as formulated, is two-dimensional. Twenty-four staves of the transducer are active (radiating); the remaining forty-eight staves are rigid. The active staves are phased to a straight line and have a cosine amplitude shading. The stave width is approximately one-half the wavelength at the transmitting frequency. The equations describing the sound pressure field inside and outside the dome as a result of the radiation of the transducer are given in Appendix A. The complete development of the analytical model can be found in Ref. 1. The equations given in Appendix A are used to compute the various performance criteria studied in this memorandum.

B. Performance Criteria

The dome-transducer performance criteria which are considered in this memorandum are defined as follows:

1. Directivity Index

A two-dimensional Directivity Index can be defined by the expression

$$\text{Directivity Index} = 20 \log_{10} \frac{P_{max}}{P_{avg}} , \qquad (1)$$
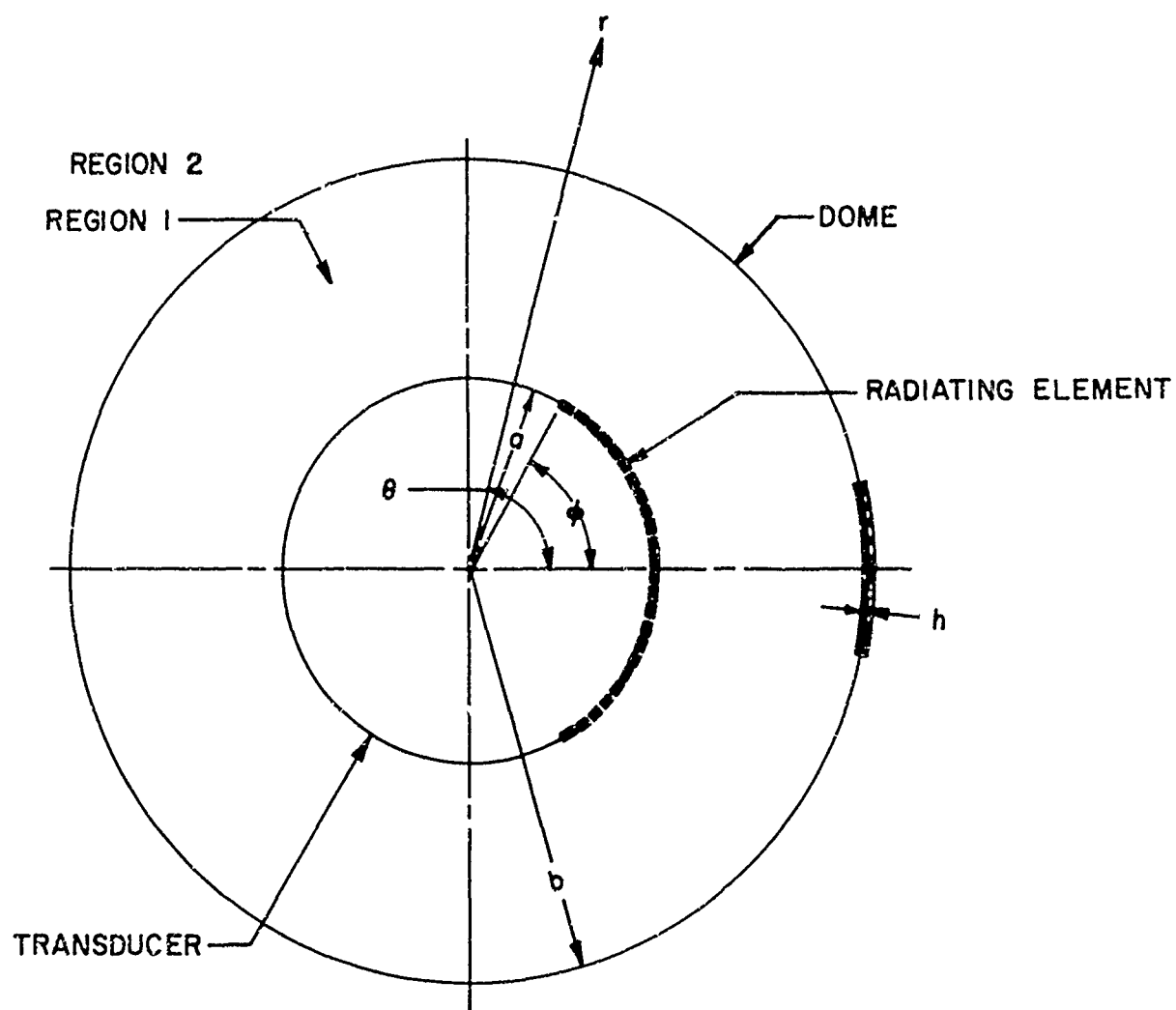
3

FIG. I – GEOMETRY FOR A CYLINDRICAL TRANSDUCER
RADIATING IN A CONCENTRIC DOME

4

where p_{max} is the maximum sound pressure in the farfield, and p_{avg} is the average sound pressure taken over 360° azimuth. The Directivity Index is computed directly from the numerical results for the farfield sound pressure field of the dome-transducer.

2. Major Lobe Width

The Major Lobe Width is defined as the width of the major lobe at the 6 dB down points of the farfield directivity pattern. Major Lobe Width is obtained directly from the numerical results for the farfield directivity pattern.

3. Side Lobe Level

Side Lobe Level is defined by the expression

$$\text{Side Lobe Level} = 20 \log_{10} \frac{p_{s\ell}}{p_{max}} , \qquad (2)$$

where $p_{s\ell}$ is the sound pressure amplitude of the <u>highest</u> side lobe in the farfield directivity pattern, and p_{max} is the maximum sound pressure amplitude in the farfield directivity pattern.

4. Dome Transmission Coefficient

Dome Transmission Coefficient is given by the expression

$$\text{Dome Transmission Coefficient} = \frac{P_t}{P_i} , \qquad (3)$$

where P_t is the time-average power transmitted through the dome, and P_i is the time-average power incident on the dome. The power incident and the power transmitted are determined by the relations

$$P_t = \text{Re} \int_0^{2\pi} p_t(r,\theta)\Big|_{r=b} \cdot v_t{}^*(r,\theta)\Big|_{r=b} \, bd\theta \quad , \qquad (4)$$

and

$$P_i = \text{Re} \int_0^{2\pi} p_i(r,\theta)\Big|_{r=b} \cdot v_i{}^*(r,\theta)\Big|_{r=b} \, bd\theta \quad , \qquad (5)$$

where $p_t(r,\theta)$ and $v_t{}^*(r,\theta)$ are respectively the sound pressure and the complex conjugate of the normal particle velocity of the sound field transmitted through the dome, and $p_i(r,\theta)$ and $v_i{}^*(r,\theta)$ are the sound pressure and the complex conjugate of the normal particle velocity of the sound field incident on the dome. These quantities (p_t, $v_t{}^*$, p_i and $v_i{}^*$) are computed as described in Appendix B. Dome Transmission Coefficient, as defined here, is primarily a function of the dome thickness and material properties and not the dome-transducer spacing. It does not measure any loss in signal level due to dome-transducer interaction, but simply the ratio of power transmitted through the dome to power incident on the dome.

    5. Dome Transfer Coefficient

        Dome Transfer Coefficient is defined by the expression

$$\text{Dome Transfer Coefficient} = 20 \log_{10}\left(\frac{P_{\text{with dome}}}{P_{\text{no dome}}}\right), \qquad (6)$$

where $P_{\text{with dome}}$[†] is the time-average power transferred to the

---

[†]$P_{\text{with dome}}$ is not equal to P_i as defined for Dome Transmission Coefficient. P_i is of arbitrary level. $P_{\text{with dome}}$ is determined from a knowledge of the transducer element velocities and the radiation loading at the transducer elements including reflections from the dome.

water by the transducer with dome, and $P_{no\ dome}$ is the time-average power transferred to the water by a bare transducer. If it is assumed that element velocity control exists in the transducer, i.e., the head velocities of the transducer elements are independent of radiation impedance, it is permissible to compare the power transferred to the water with and without the dome. (If velocity control does not exist, the analysis becomes much more complex, the head velocity for each element must be obtained by solving a large set of simultaneous equations. Absence of velocity control can effect a degradation of sonar performance.) The power P transferred is given by the expression

$$P = Re \int_{-\pi}^{\pi} p(r,\theta)|_{r=a} \cdot v^*(r,\theta)|_{r=a} \, ad\theta \quad , \tag{7}$$

where $p(r,\theta)$ is the sound pressure, and $v^*(r,\theta)$ is the complex conjugate of the normal particle velocity. Both $p(r,\theta)$ and $v^*(r,\theta)$ are obtained from the expressions given in Appendix A. The integral is taken over the transducer face. (See Fig. 1.) Dome Transmission Coefficient measures that fraction of incident energy which is transmitted through the dome. The remainder of the energy is reflected from the dome. Dome Transfer Coefficient is a measure of the manner in which the reflected energy interferes with the transducer.

6. Nearfield Roughness

Nearfield Roughness is defined by the expression

$$\text{Nearfield Roughness} = 20 \log_{10} \frac{\bar{P}_{max}}{\bar{P}_{mean}} \quad , \tag{8}$$

where $\bar{P}_{max}$ is the maximum pressure amplitude, and $\bar{P}_{mean}$ is the mean pressure amplitude on the active portion of the transducer

7

face. Nearfield Roughness is obtained directly from the numerical
evaluation of the nearfield sound pressure of the dome-transducer
model.

C. Parameters of the Dome-Transducer Model

The parameters of the dome-transducer model and their
dimensions are given in the table below.

PARAMETER	SYMBOL	DIMENSION[*]
Transducer Radius	a	L
Dome Radius	b	L
Dome Thickness	h	L
Sound Velocity in the fluid	c	LT^{-1}
Density of the fluid	ρ	ML^{-3}
Operating wavelength in the fluid	λ	L
Plate Modulus of dome material	E_s[+]	$ML^{-1}T^{-2}$
Density of dome material	ρ_s	ML^{-3}

---

[*]Dimensions are given in the mass, length, time system with
dimensions M, L, T respectively.

[+]$E_s = \dfrac{E}{(1-\gamma^2)}$; E is Young's Modulus, γ is Possion's Ratio

In order to cover a practical range of sonar applications,
it is necessary to evaluate the various performance criteria for
a wide range of values for the dome-transducer parameters. The
direct presentation of this data would require considerable space
and be quite cumbersome to apply directly to a design problem.
Furthermore, trends in the data would be difficult to recognize.
The problem of data presentation is simplified considerably by

grouping the dome-transducer parameters in <u>dimensionless</u> products.[*]
Performance criteria then can be displayed as functions of the
dimensionless products. This procedure enables the designer to
recognize trends in the data, and the volume of data is reduced
to a set of compact curves which can be used efficiently. Apply-
ing the methods of dimensional analysis,[2] using some insight,
and performing a few trial and error calculations leads one to
adopt the following dimensionless products:

1. h/λ, dome thickness product

2. $(b-a)/\lambda$, dome-transducer spacing product

3. $E_s/\rho c^2$, dome stiffness product

4. ρ_s/ρ, dome density product.

The product $2a/\lambda$, the ratio of transducer diameter to
wavelength, and the above products form a complete set of
dimensionless products. Typical values of $2a/\lambda$ for current
sonar systems range between 8 and 12. A nominal value of 11
was used for the computations included in this technical memo-
randum. Results for other values of $\frac{2a}{\lambda}$ in the range 8-12 will
be similar qualitatively to the results presented here.

---

[*]The word "product" will be used to denote <u>dimensionless</u> groupings
of the <u>dimensioned</u> system parameters (h, λ, etc.).

III.   RESULTS

This section contains numerical results which demonstrate
the dependence of performance criteria on the dimensionless
products of the dome-transducer model. Linear plots, most of
which have the thickness product h/λ as the independent variable,
are employed to present the performance criteria data. Each plot
contains a family of curves generated by varying one of the
dimensionless products while the other two products remain
constant. The range of values of the dimensionless products is
chosen to span the areas of current interest and demonstrate the
behavior of each performance criterion. The ranges of the
dimensionless products are

DIMENSIONLESS PRODUCT	RANGE OF VALUES
h/λ	$0.0 \rightarrow 0.0365$
$(b-a)/\lambda$	$1.5, 2.0, 3.0$
ρ_s/ρ	$2.0, 3.9, 7.9$
$E_s/\rho c^2$	$90, 90 \times 10^{-2}, 90 \times 10^{-4}$

The thickness product, h/λ, spans the practical limits of metal
and, possibly, plastic domes. The range of $(b-a)/\lambda$ brackets the
minimum and maximum dome-transducer separation of the AN/SQS-4,
AN/SQS-23, and AN/SQS-26 systems. Values of the density product,
ρ_s/ρ, include steel, plastic, and some wire-reinforced rubber
compounds. The stiffness product, $E_s/\rho c^2$, has a range which
covers most practical metals and some plastics. Approximate
values of the dimensionless products for a system such as the
AN/SQS-26 are $h/\lambda = 0.02$, $(b-a)/\lambda = 2.0$, $\rho_s/\rho = 7.9$, and $E_s/\rho c^2 = 90$ (metal dome).

Typically, a set of three plots is shown for each perform-
ance criterion. In the first plot, density product ρ_s/ρ and

stiffness product $E_s/\rho c^2$ are constant; spacing product $(b-a)/\lambda$ is varied to produce the family of curves. Values of density product ρ_s/ρ are shown in the second plot for constant values of stiffness product $E_s/\rho c^2$ and spacing product $(b-a)/\lambda$. The third plot is generated with different values of stiffness product $E_s/\rho c^2$ for constant ρ_s/ρ and $(b-a)/\lambda$.

A. Directivity Index

Directivity Index is displayed in Figs. 2, 3, and 4. Data in Fig. 2 indicate decreasing directivity for increased values of the spacing product $(b-a)/\lambda$ and the thickness product h/λ. The effect of the $(b-a)/\lambda$ is less pronounced than the effect produced by h/λ. Figure 3 shows the improved directivity produced by lower values of the density product ρ_s/ρ. As shown in Fig. 4, the present range of the stiffness product $E_s/\rho c^2$ has no effect on Directivity Index.

B. Major Lobe Width

Results for Major Lobe Width are shown in Figs. 5, 6, and 7. Major Lobe Width increases as a function of the thickness product h/λ but decreases as a function of the spacing product $(b-a)/\lambda$ for the large density product ρ_s/ρ as shown in Fig. 5. However, for small ρ_s/ρ no dependence is seen on either h/λ or $(b-a)/\lambda$ as shown in Fig. 6. Results in Fig. 7 indicate that Major Lobe Width is independent of the stiffness product $E_s/\rho c^2$.

C. Side Lobe Level

Data for Side Lobe Level are given in Figs. 8, 9, and 10. The effects of the spacing product $(b-a)/\lambda$ and the thickness product h/λ for the constant density product ρ_s/ρ and the stiffness product $E_s/\rho c^2$ are shown in Fig. 8. The level of the side lobes increases for increasing values of h/λ and $(b-a)/\lambda$. From Fig. 9, reduced values of density product, ρ_s/ρ, appear to produce side lobes which are lower than those of a bare transducer. However, as shown in the farfield directivity patterns in Figs.

11

11 and 12, this phenomenon is associated with the presence of
two, nearly equal, side lobes, and what appears as an improve-
ment, actually compounds the problem. Doubling of the side lobes
appears to occur for values of $(b-a)/\lambda$ of 1.5 - 2.5 . Figure 10
adds data indicating the independence of Side Lobe Level on the
stiffness product $E_s/\rho c^2$.

D. Dome Transmission Coefficient

Figures 13, 14, and 15 display results for Dome Trans-
mission Coefficient. Figures 13 and 15 show transmission to
be independent of the spacing product $(b-a)/\lambda$ and the stiffness
product $E_s/\rho c^2$. Strong dependence on the density product is
shown in Fig. 14. For values of the density product ρ_s/ρ
approaching unity, transmission becomes independent of all
products, as expected.

E. Dome Transfer Coefficient

In Figs. 16, 17, and 18, Dome Transfer Coefficient
is plotted with the spacing product $(b-a)/\lambda$ as the independent
variable. The data show Dome Transfer Coefficient to be a damped,
periodic function of $(b-a)/\lambda$, with period $\lambda/2$. This behavior
is attributed to strong standing waves set up in the dome-
transducer model. The standing wave patterns in real domes
should not be so pronounced; however, such geometry effects
cannot be completely ignored. Analytical models with more
realistic geometry will yield better determinations of the
effects of system geometry on performance.

F. Nearfield Roughness

Results for Nearfield Roughness are presented in
Figs. 19, 20, and 21. Figures 19 and 21 show Nearfield Roughness
to be independent of the spacing product $(b-a)/\lambda$ and the stiffness
product $E_s/\rho c^2$. In Fig. 20 an increase in Nearfield Roughness
is noted for $\rho_s/\rho > 2.0$. For smaller values of the density
product ρ_s/ρ Nearfield Roughness appears to be independent of
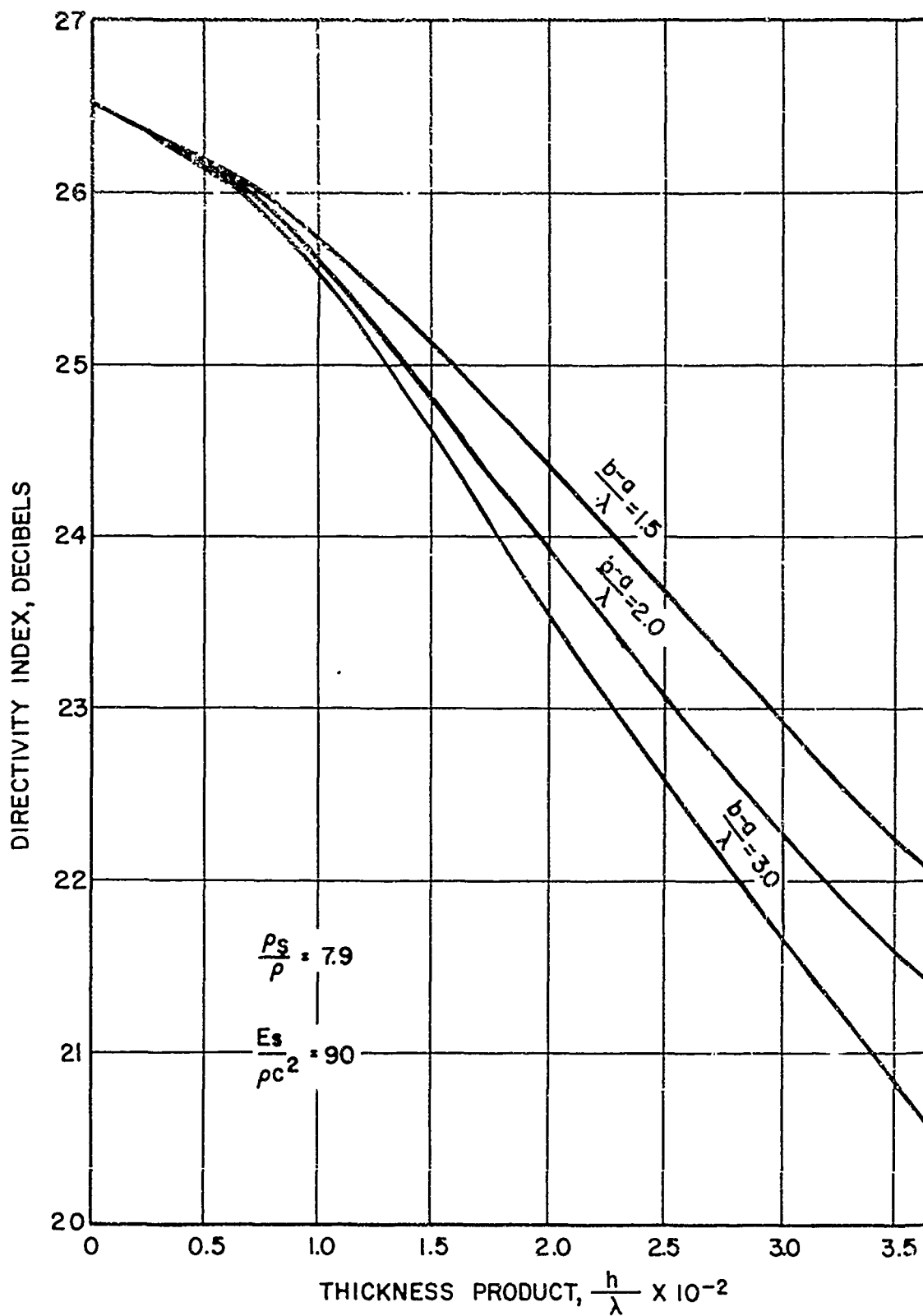all dimensionless products.

FIG. 2—DIRECTIVITY INDEX VS THICKNESS PRODUCT, $\frac{h}{\lambda}$ FOR FIXED DENSITY PRODUCT $\frac{\rho_s}{\rho}$ AND STIFFNESS PRODUCT $\frac{E_s}{\rho c^2}$
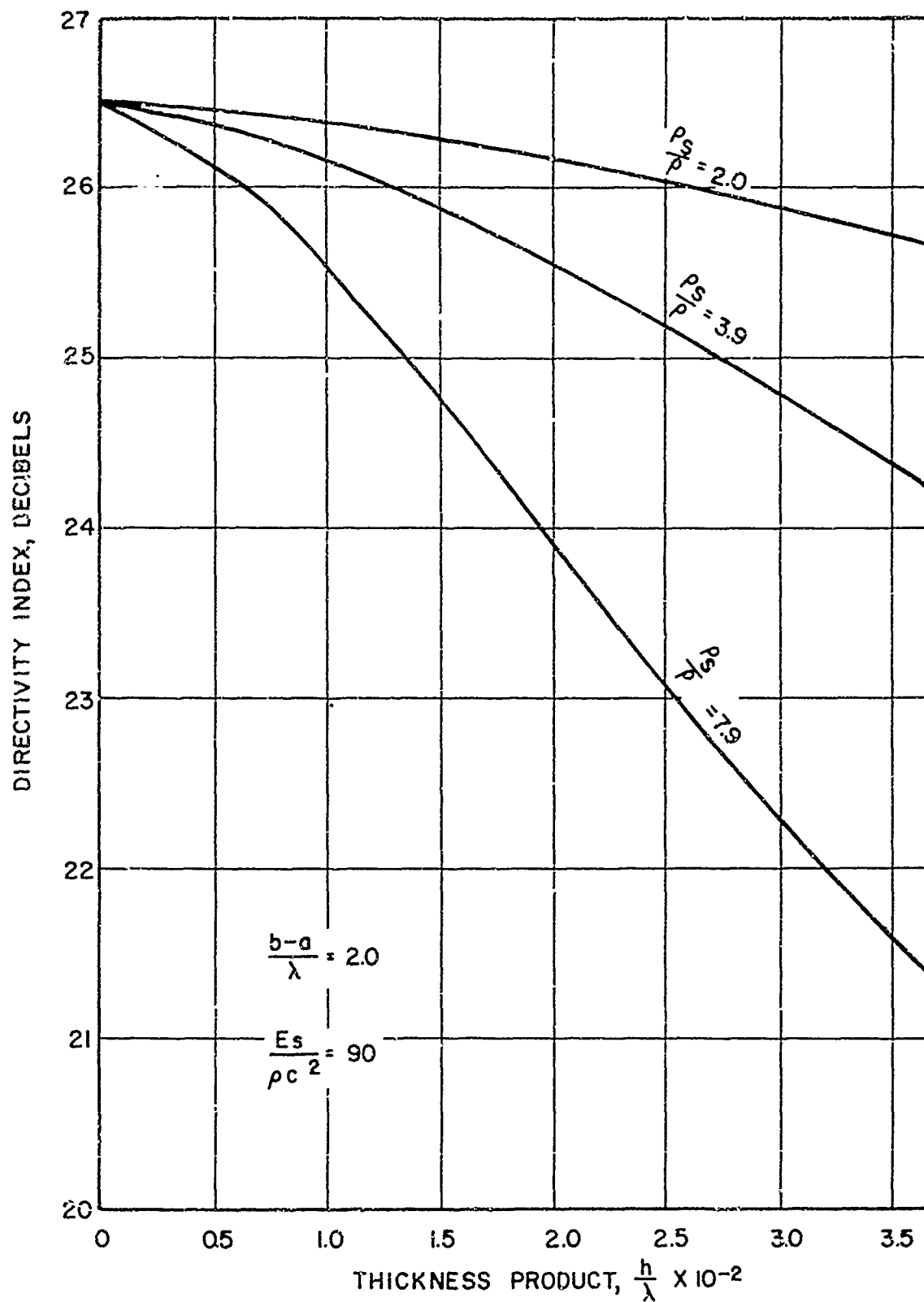
13

FIG.3 – DIRECTIVITY INDEX VS. THICKNESS PRODUCT $\frac{h}{\lambda}$. FOR FIXED SEPARATION PRODUCT $\frac{b-a}{\lambda}$ AND STIFFNESS PRODUCT $\frac{Es}{\rho c^2}$
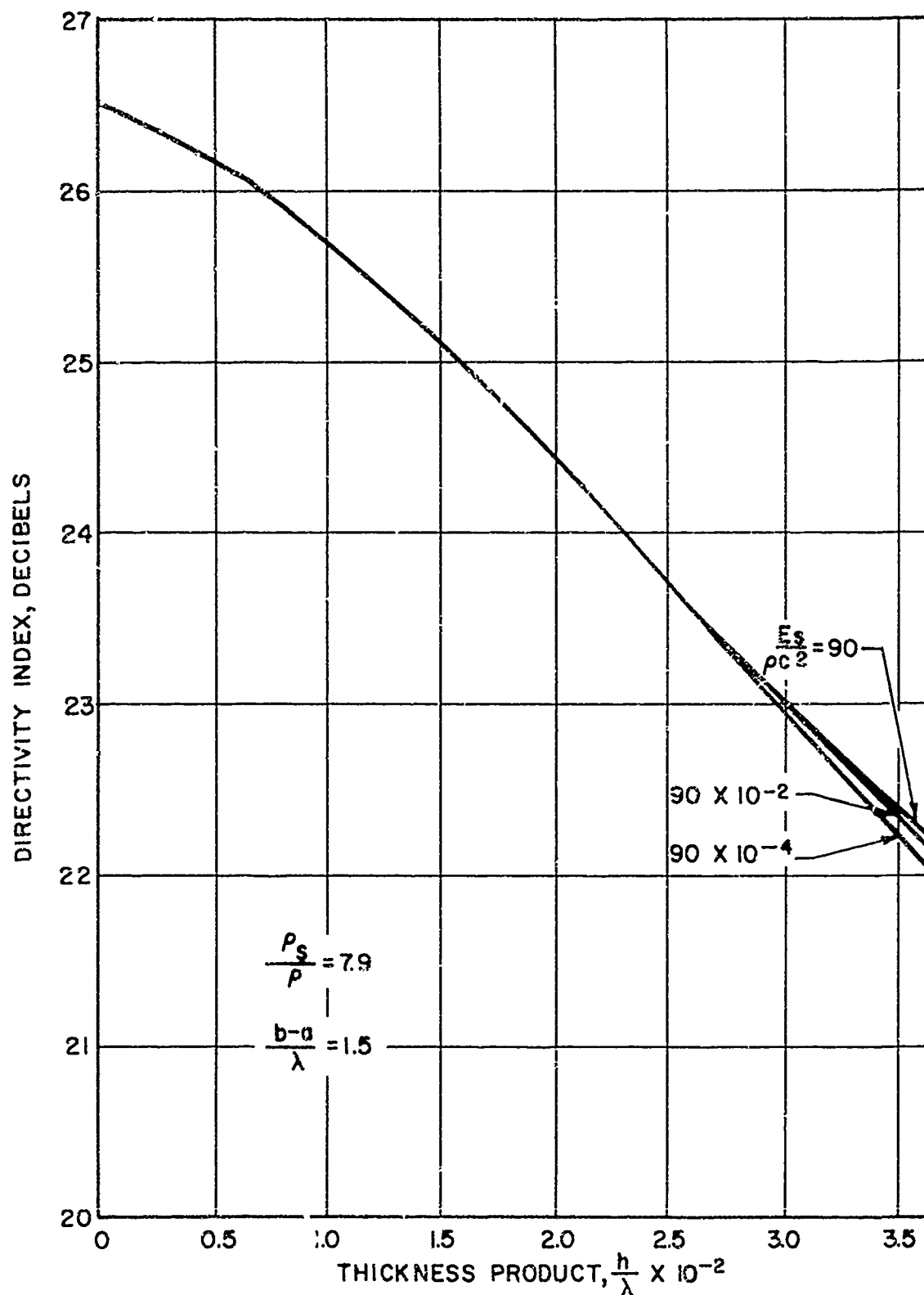
14

FIG. 4—DIRECTIVITY INDEX VS
THICKNESS PRODUCT $\frac{h}{\lambda}$ FOR
FIXED DENSITY PRODUCT $\frac{\rho_s}{\rho}$
AND SEPARATION PRODUCT $\frac{b-a}{\lambda}$

15

FIG. 5—MAJOR LOBE WIDTH VS
THICKNESS PRODUCT $\frac{h}{\lambda}$
FOR FIXED DENSITY PRODUCT $\frac{\rho_s}{\rho}$
AND STIFFNESS PRODUCT $\frac{E_s}{\rho c^2}$

16

FIG. 6 –MAJOR LOBE WIDTH VS
THICKNESS PRODUCT $\frac{h}{\lambda}$
FOR FIXED SEPARATION PRODUCT $\frac{b-a}{\lambda}$
AND STIFFNESS PRODUCT $\frac{Es}{\rho c^2}$

17

FIG. 7 — MAJOR LOBE WIDTH VS
THICKNESS PRODUCT $\frac{h}{\lambda}$ FOR
FIXED DENSITY PRODUCT $\frac{\rho_s}{\rho}$
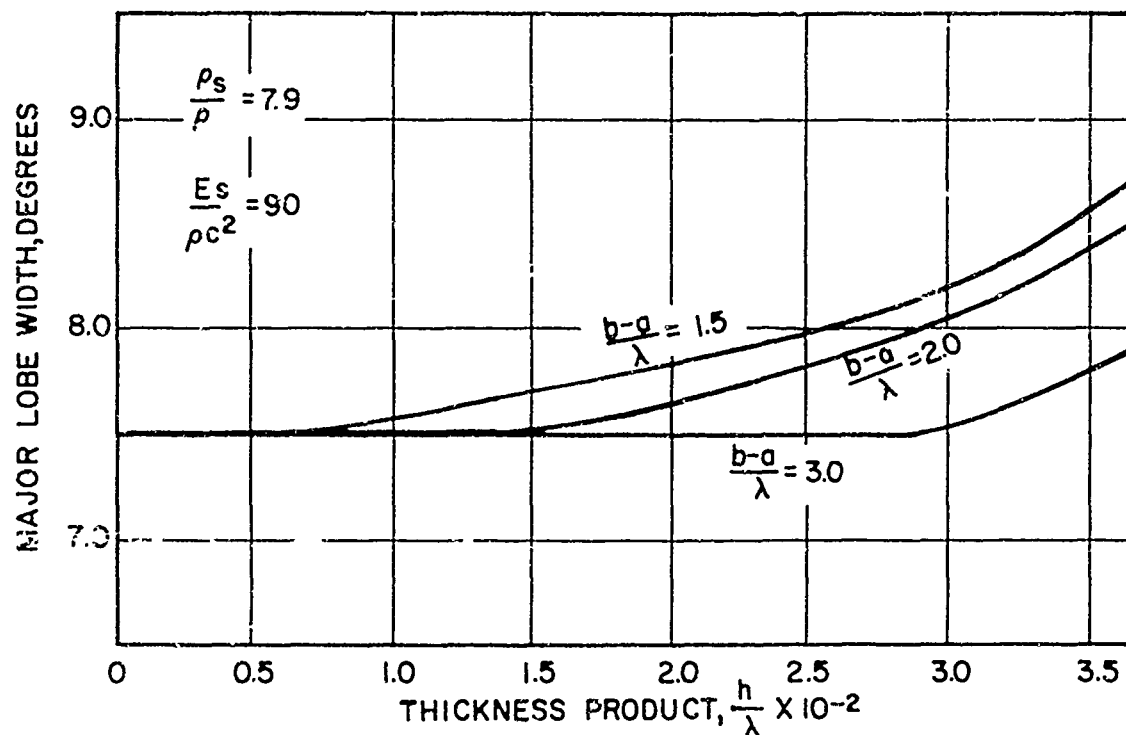AND SEPARATION PRODUCT $\frac{b-a}{\lambda}$

18

FIG. 8 — SIDE LOBE LEVEL VS THICKNESS PRODUCT $\frac{h}{\lambda}$ FOR FIXED DENSITY PRODUCT $\frac{\rho_s}{\rho}$ AND STIFFNESS PRODUCT $\frac{E_s}{\rho c^2}$
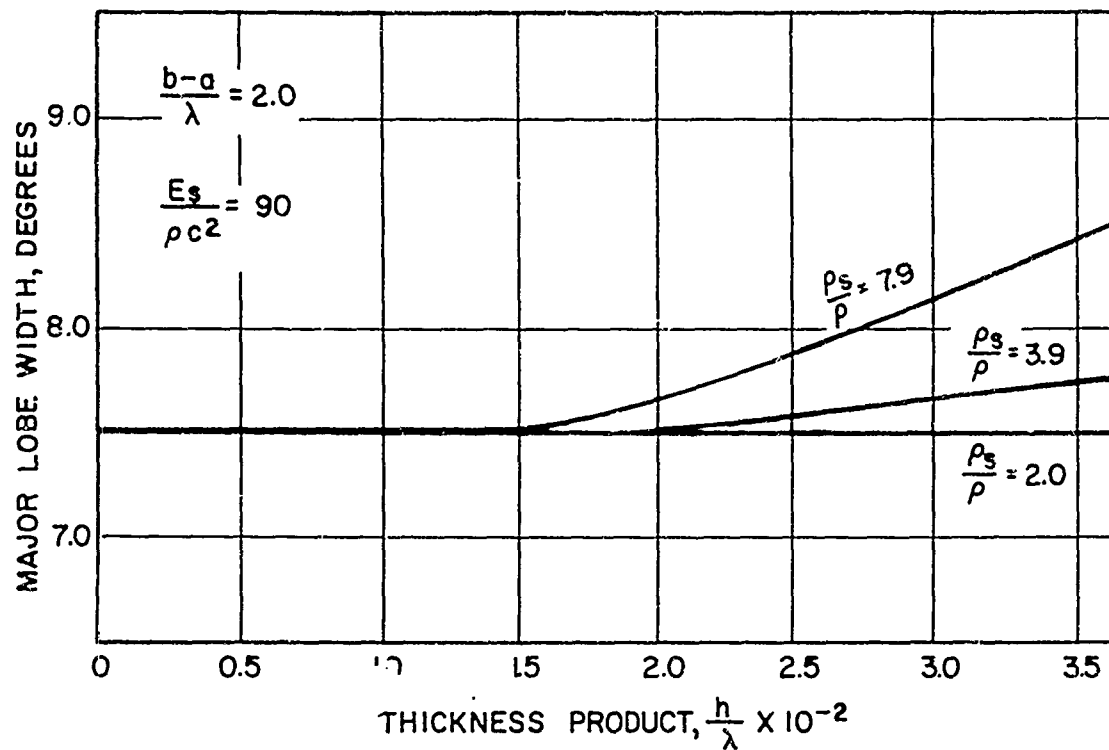
19

FIG. 9—SIDE LOBE LEVEL VS THICKNESS
PRODUCT $\frac{h}{\lambda}$ FOR FIXED SEPARATION
PRODUCT $\frac{b-a}{\lambda}$ AND
STIFFNESS PRODUCT $\frac{Es}{\rho c^2}$

20

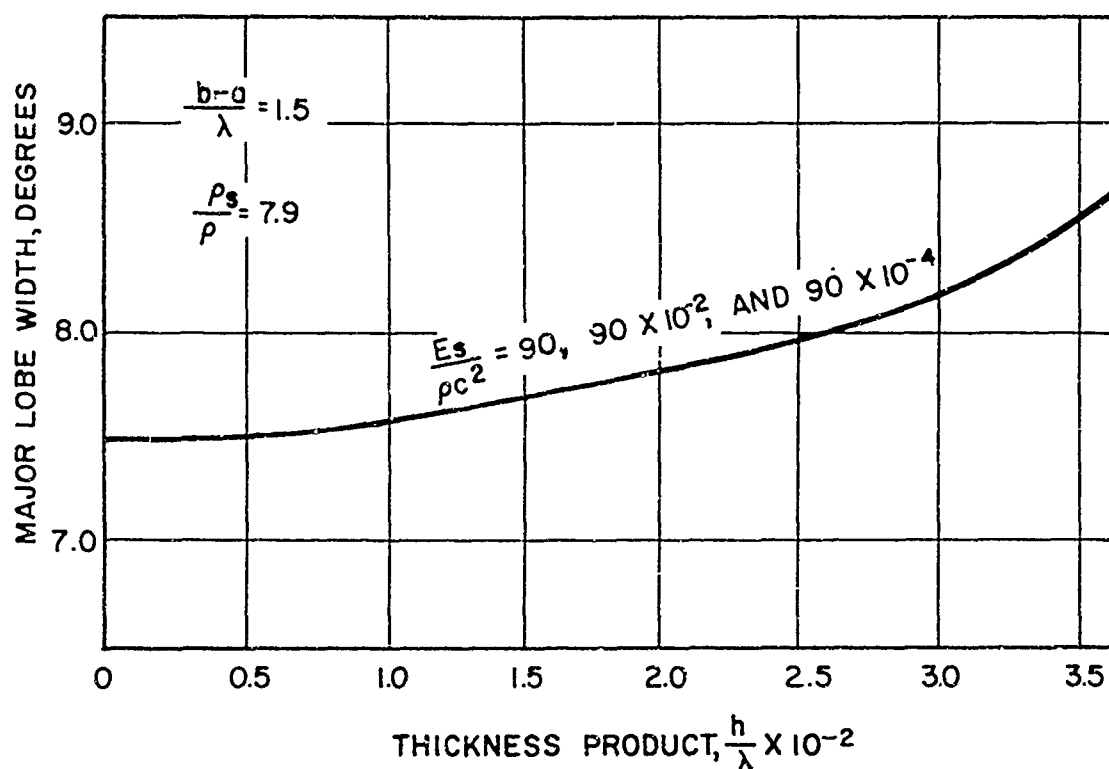TRACOR, INC.   I   DWG. 6534
AUSTIN, TEXAS   12/21/65   JDM/SL

FIG. 10 — SIDE LOBE LEVEL VS THICKNESS PRODUCT $\frac{h}{\lambda}$ FOR FIXED DENSITY PRODUCT $\frac{\rho s}{\rho}$ AND SEPARATION PRODUCT $\frac{b-a}{\lambda}$
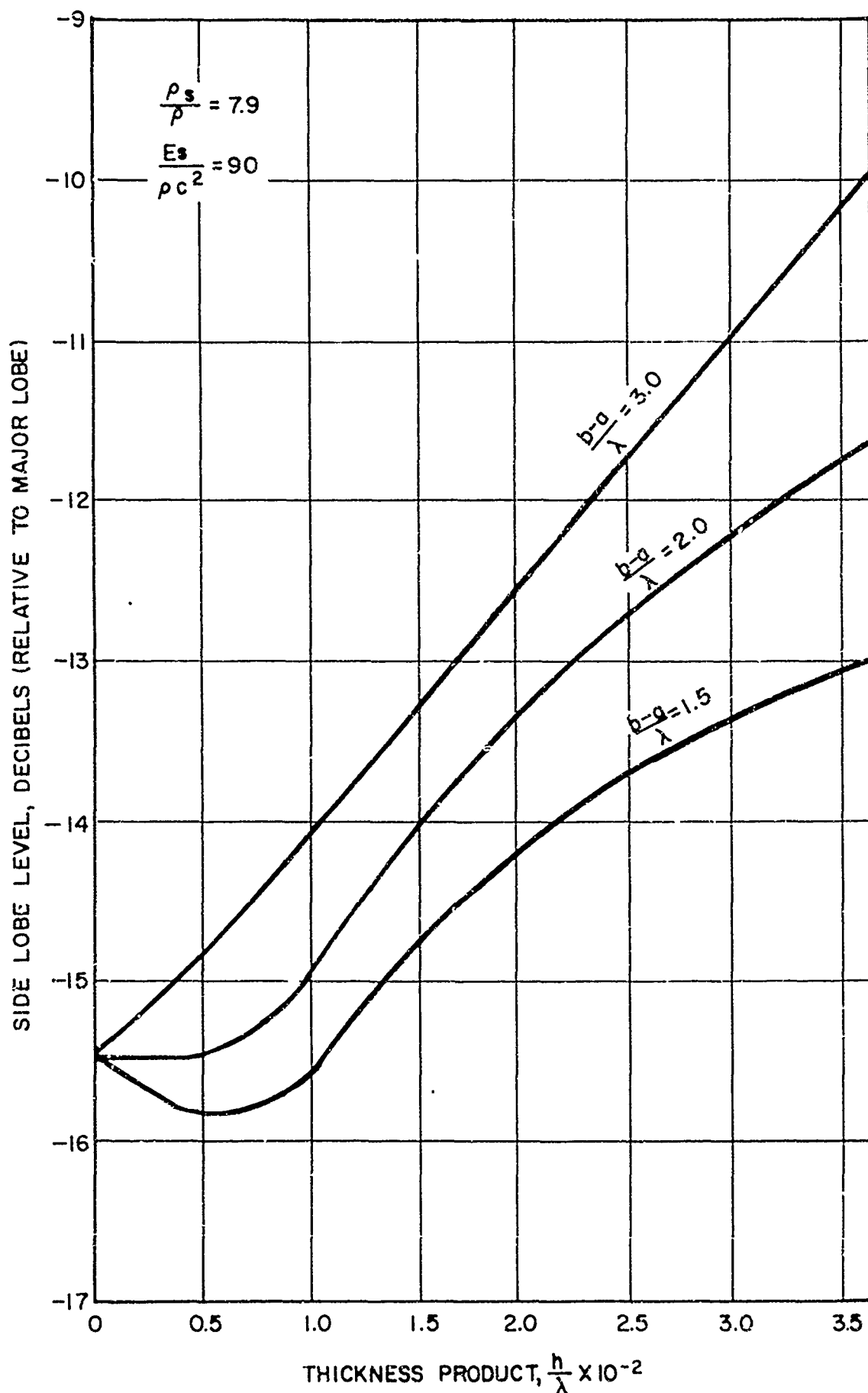
21

FIG. 11 – FARFIELD DIRECTIVITY PATTERN, DECIBELS

$$\frac{b-a}{\lambda} = 1.5 \qquad\qquad \frac{h}{\lambda} = 2.19 \times 10^{-2}$$

$$\frac{Es}{\rho c^2} = 90 \qquad\qquad \frac{\rho_s}{\rho} = 3.9$$

22

FIG. 12 — FARFIELD DIRECTIVITY PATTERN, DECIBELS

$$\frac{b-a}{\lambda} = 1.5$$

$$\frac{Es}{\rho c^2} = 90$$

$$\frac{h}{\lambda} = 2.19 \times 10^{-2}$$

$$\frac{\rho s}{\rho} = 2.0$$

23
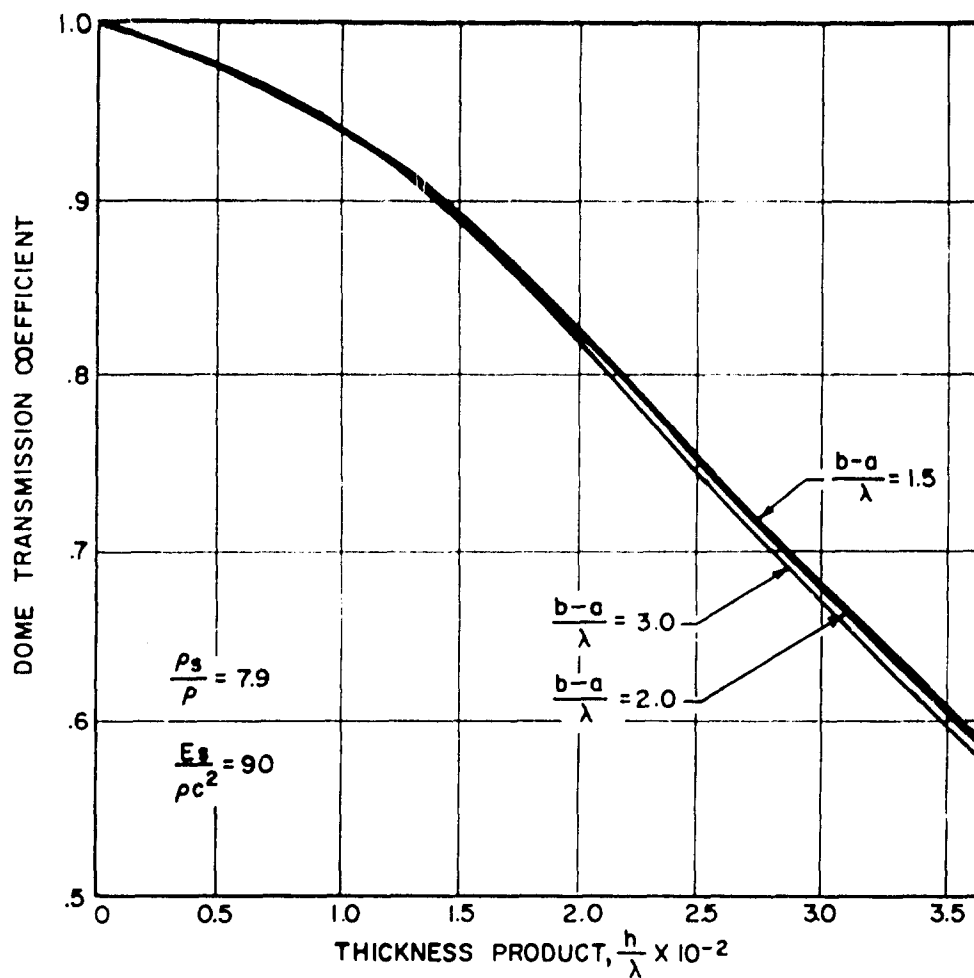
FIG. 13— DOME TRANSMISSION COEFFICIENT VS
THICKNESS PRODUCT $\frac{h}{\lambda}$ FOR FIXED DENSITY
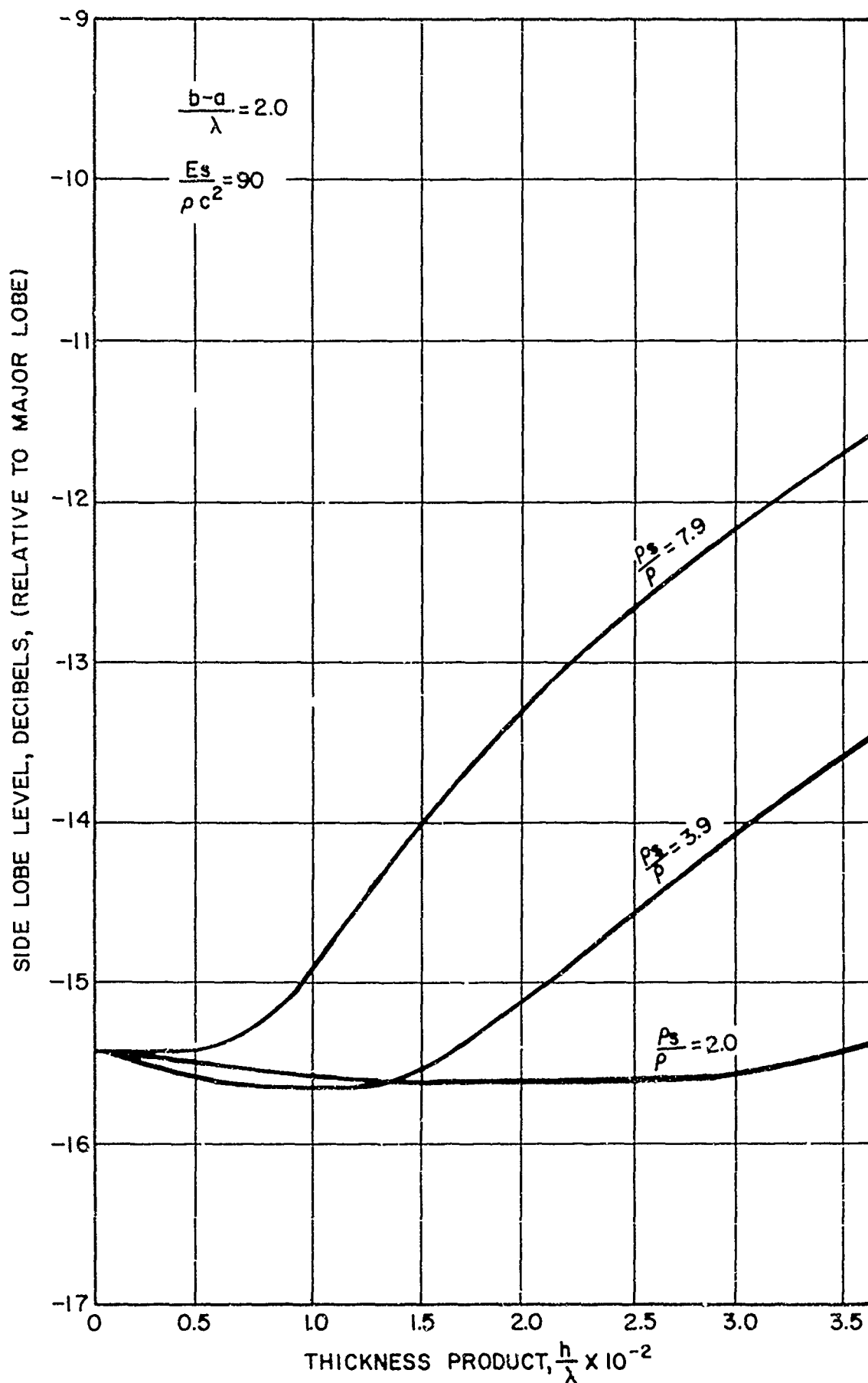PRODUCT $\frac{\rho s}{\rho}$ AND STIFFNESS PRODUCT $\frac{E s}{\rho c^2}$

24

FIG. 14—DOME TRANSMISSION COEFFICIENT VS
THICKNESS PRODUCT $\frac{h}{\lambda}$ FOR FIXED SEPARATION
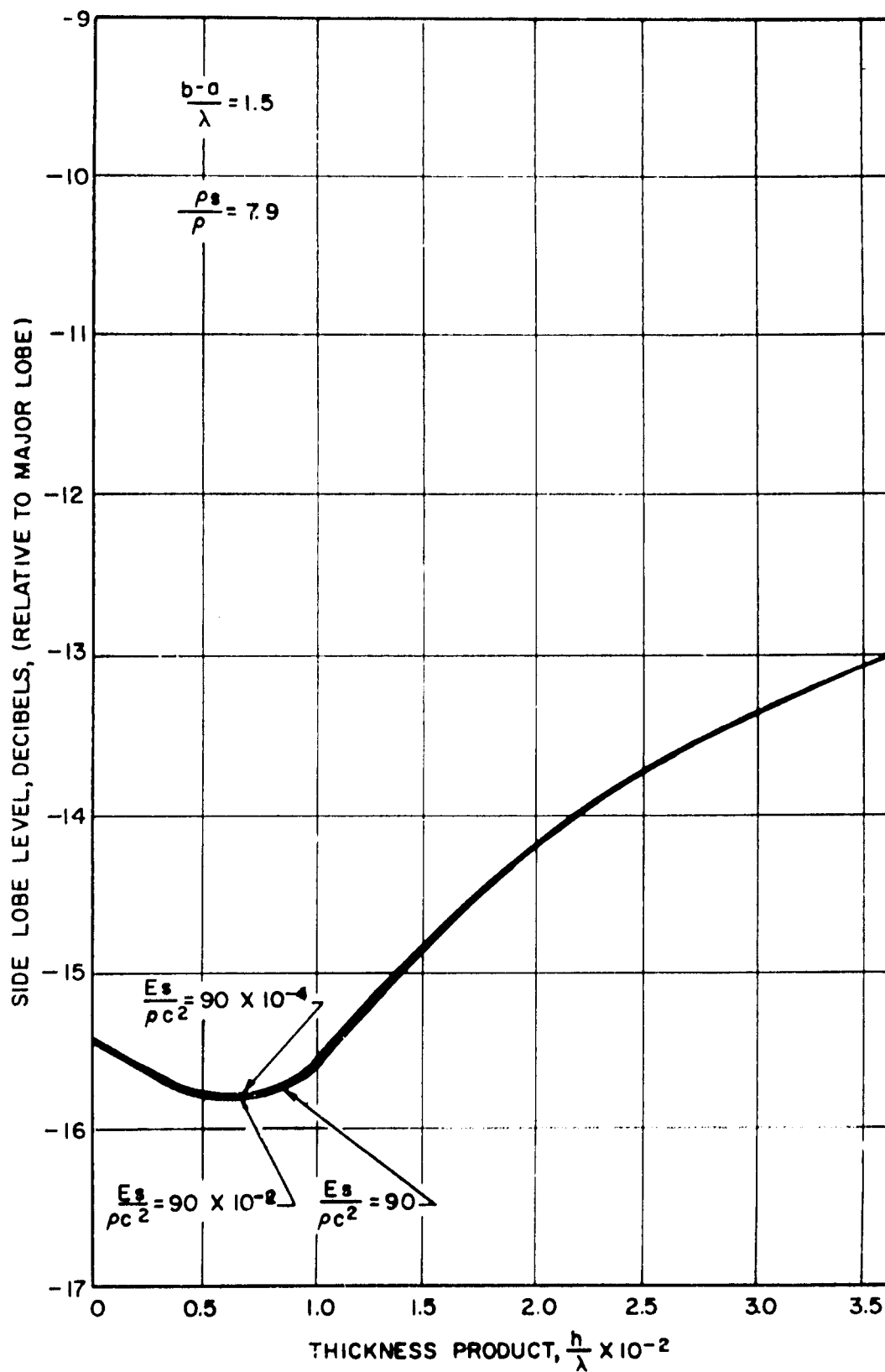PRODUCT $\frac{b-a}{\lambda}$ AND STIFFNESS PRODUCT $\frac{Es}{\rho c^2}$

25

FIG.15−DOME TRANSMISSION COEFFICIENT VS
THICKNESS PRODUCT $\frac{h}{\lambda}$ FOR FIXED DENSITY
PRODUCT $\frac{\rho_s}{\rho}$ AND SEPARATION PRODUCT $\frac{b-a}{\lambda}$

26

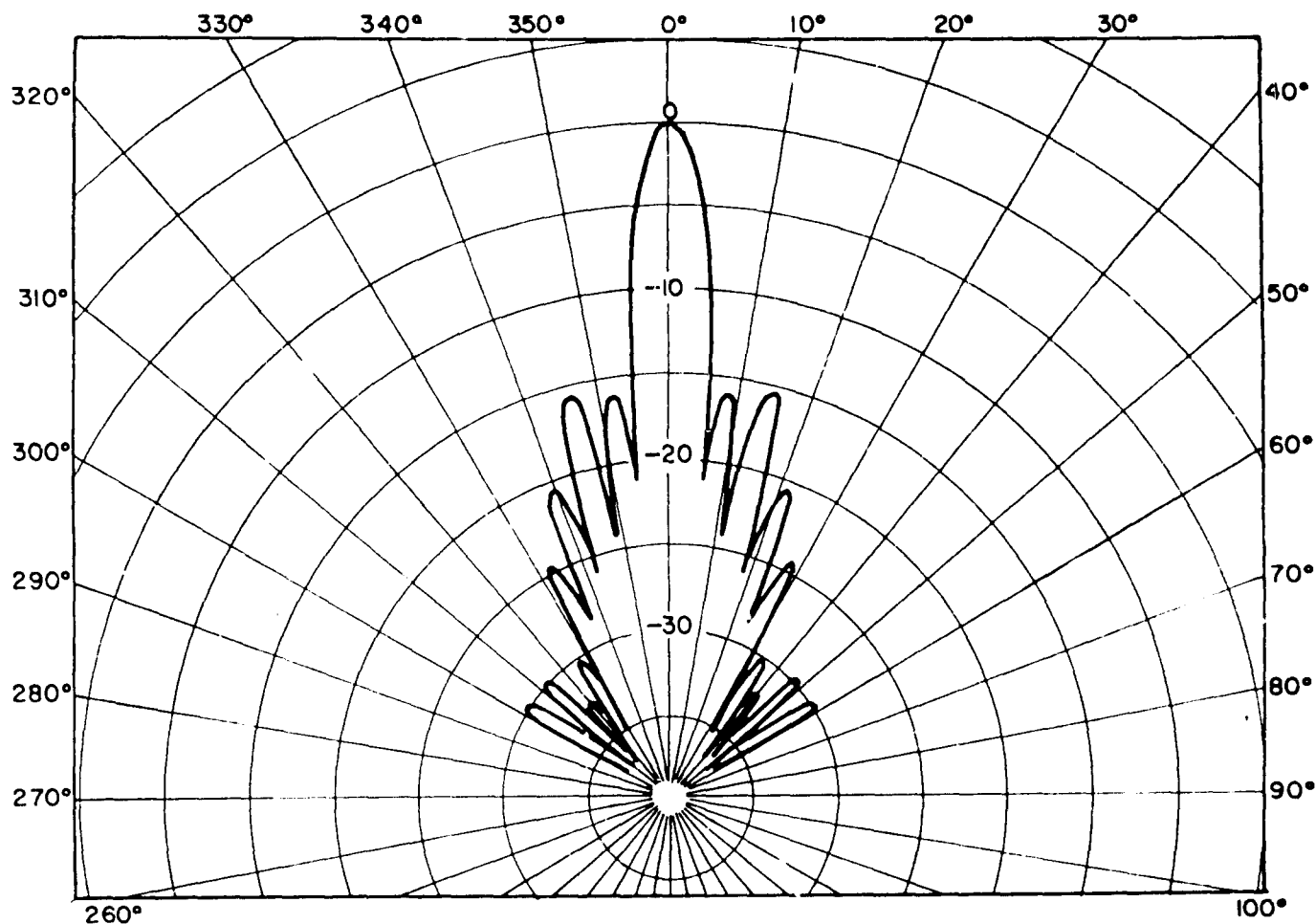FIG.16—DOME TRANSFER COEFFICIENT VS
SEPARATION PRODUCT $\frac{b-a}{\lambda}$ FOR FIXED
DENSITY PRODUCT $\frac{\rho_s}{\rho}$ AND STIFFNESS
PRODUCT $\frac{Es}{\rho c^2}$
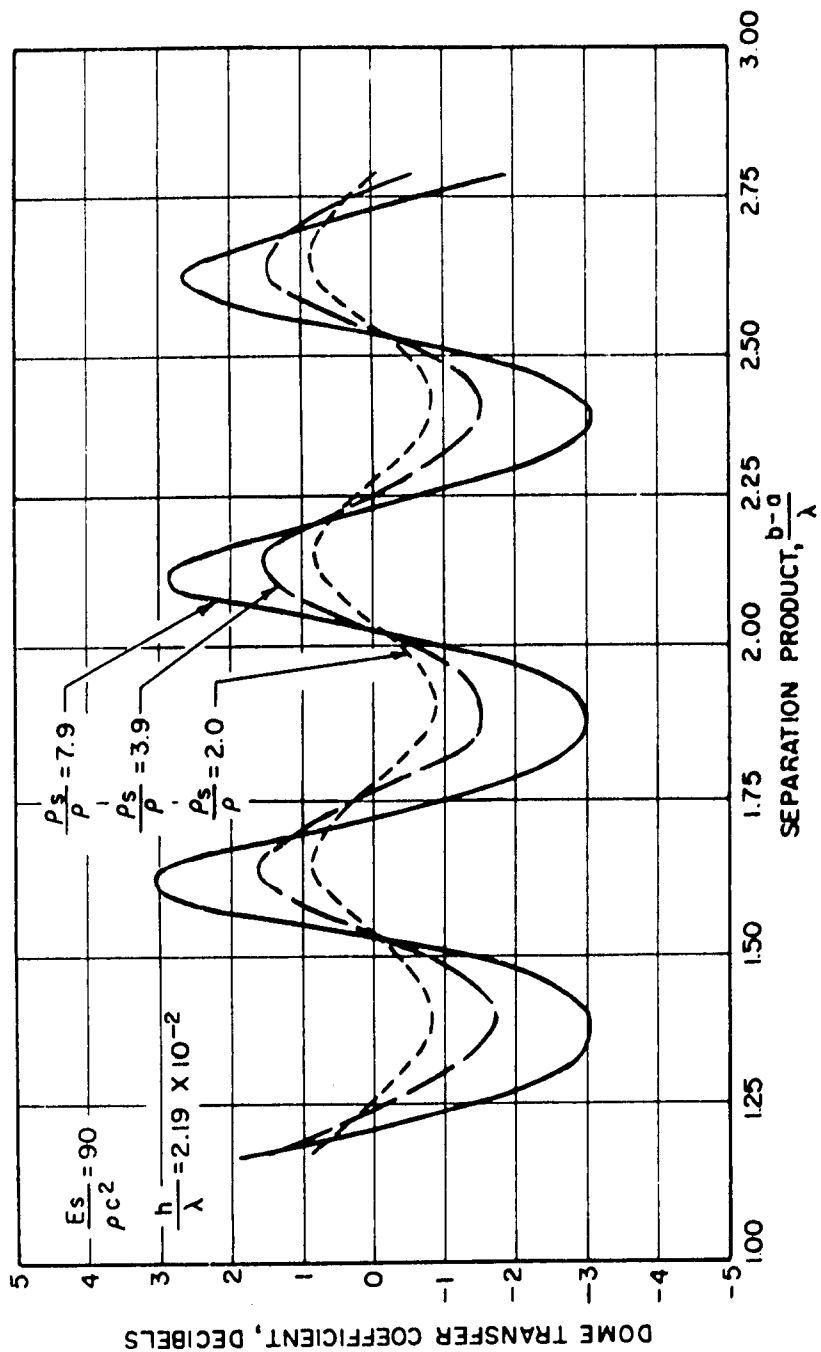
FIG. 17–DOME TRANSFER COEFFICIENT VS SEPARATION PRODUCT $\frac{b-a}{\lambda}$ FOR FIXED STIFFNESS PRODUCT $\frac{Es}{\rho c^2}$ AND THICKNESS PRODUCT $\frac{h}{\lambda}$

28
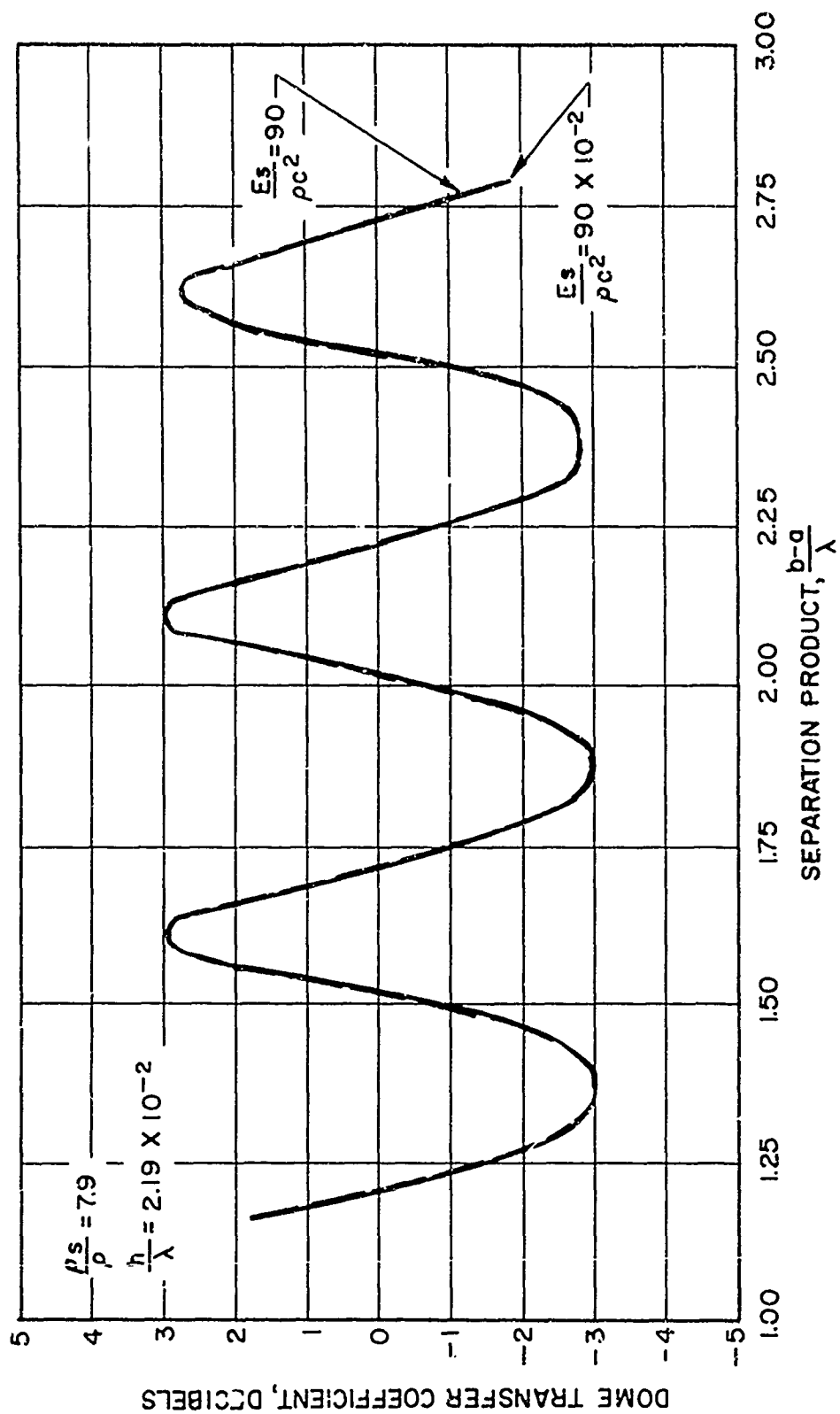
FIG. 18—DOME TRANSFER COEFFICIENT VS
SEPARATION PRODUCT $\frac{b-a}{\lambda}$ FOR FIXED
DENSITY PRODUCT $\frac{\rho s}{\rho}$ AND
THICKNESS $\frac{h}{\lambda}$

FIG. 19—NEARFIELD ROUGHNESS VS
THICKNESS PRODUCT $\frac{h}{\lambda}$ FOR FIXED
DENSITY PRODUCT $\frac{\rho s}{\rho}$ AND STIFFNESS
PRODUCT $\frac{Es}{\rho c^2}$

30
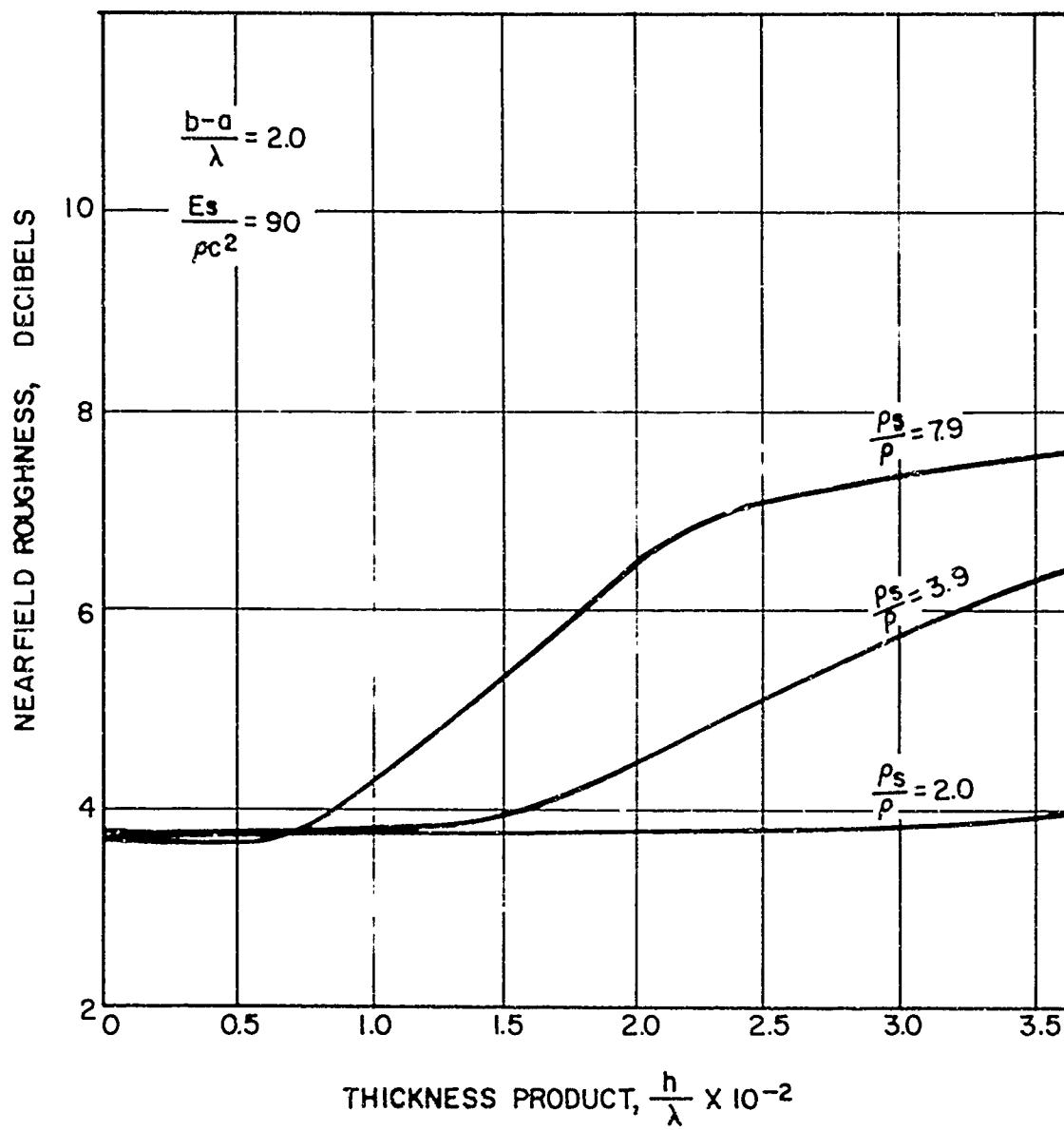
FIG. 20 — NEARFIELD ROUGHNESS VS
THICKNESS PRODUCT $\dfrac{h}{\lambda}$
FOR FIXED SEPARATION PRODUCT $\dfrac{b-a}{\lambda}$
AND STIFFNESS PRODUCT $\dfrac{Es}{\rho c^2}$

31
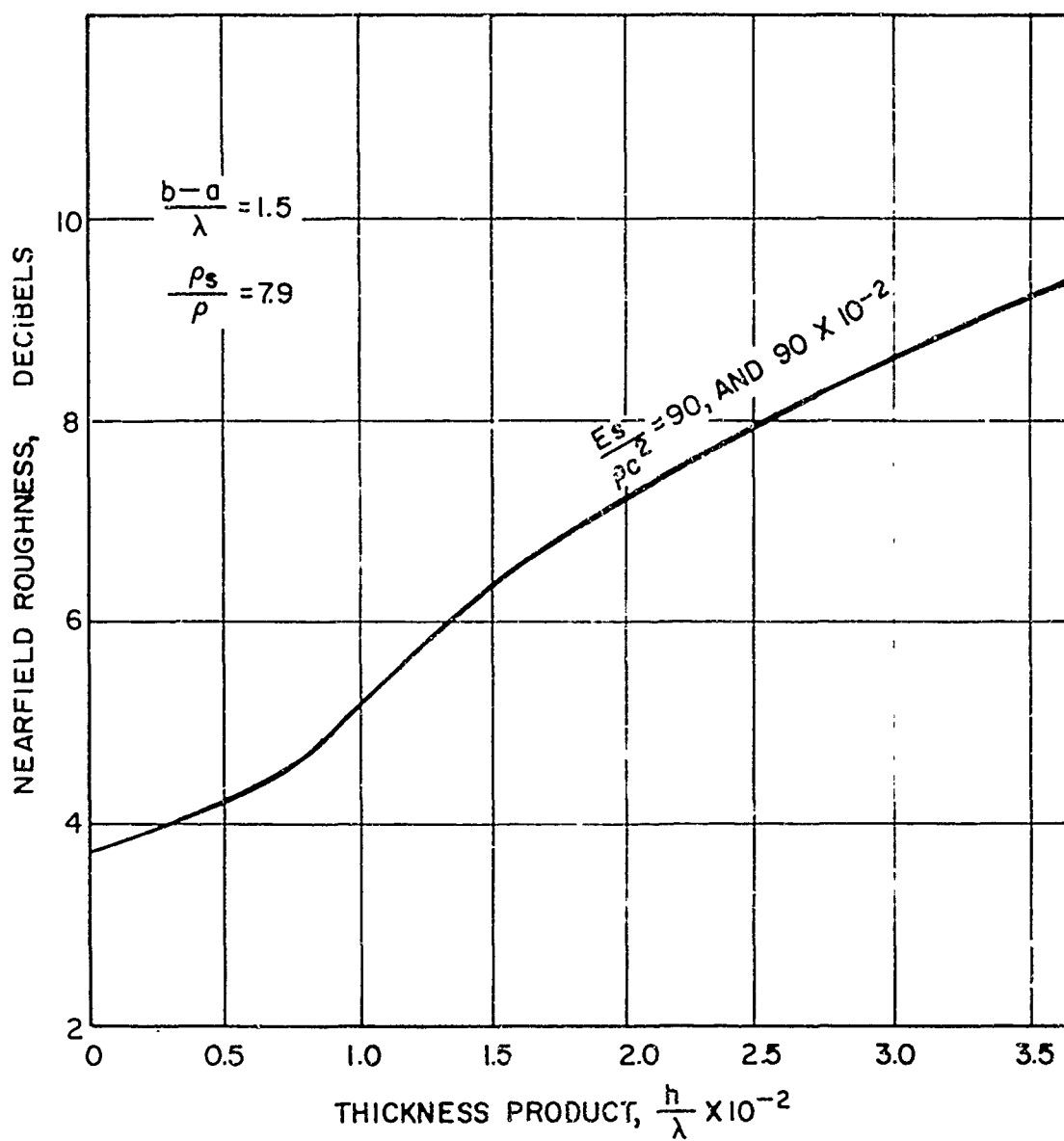
FIG. 21 – NEARFIELD ROUGHNESS VS
THICKNESS PRODUCT $\frac{h}{\lambda}$ FOR
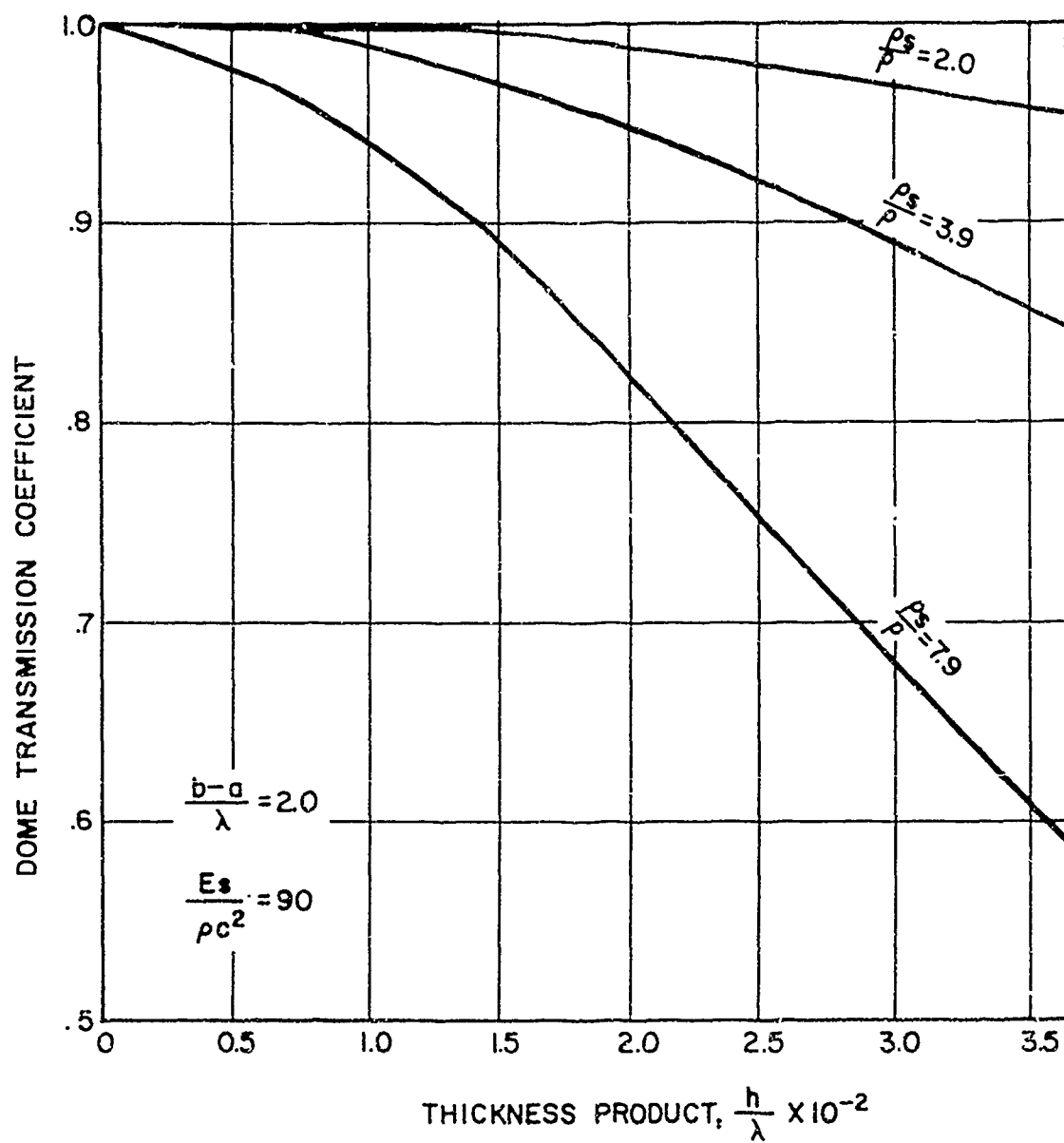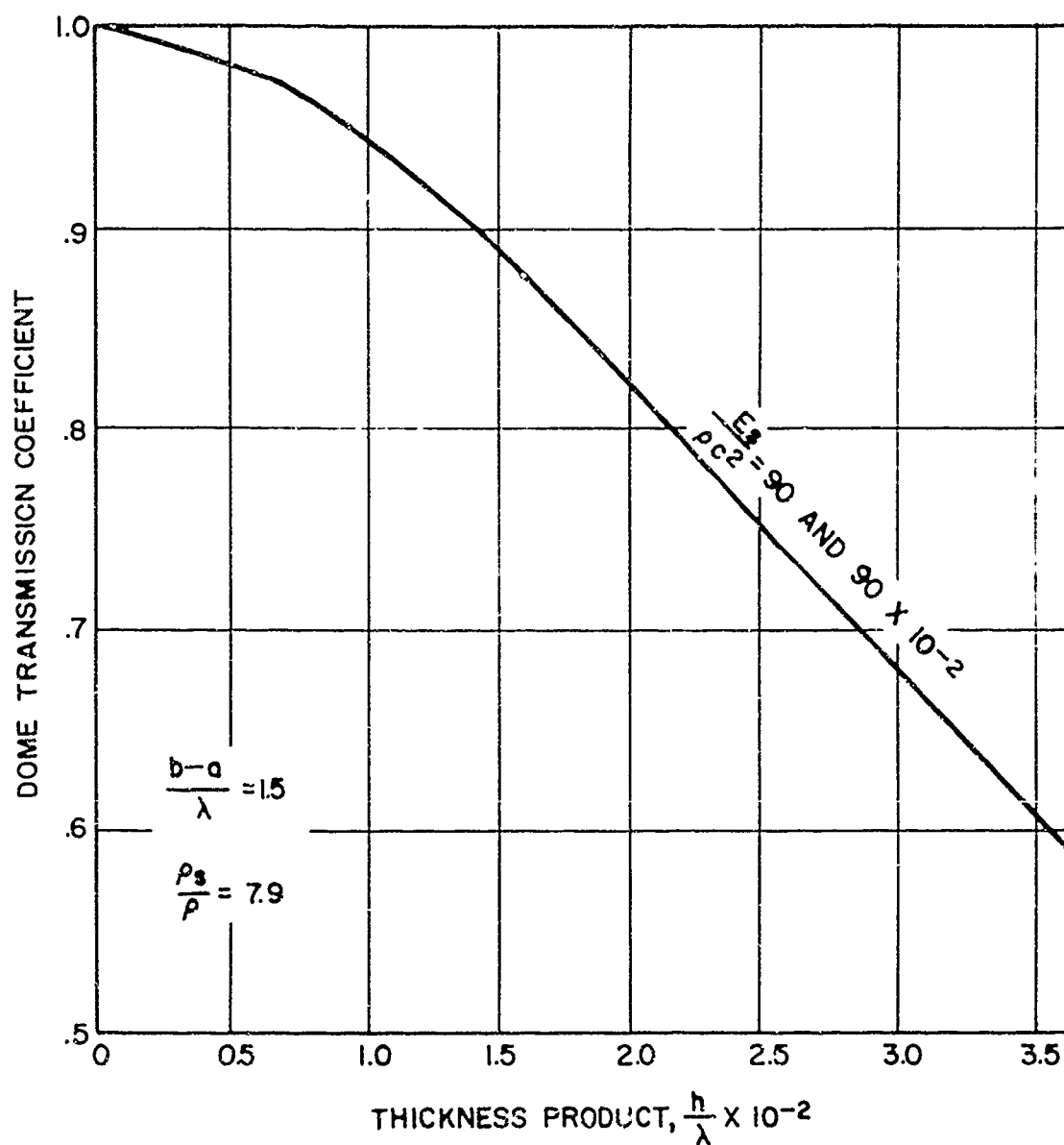FIXED DENSITY PRODUCT $\frac{\rho_s}{\rho}$
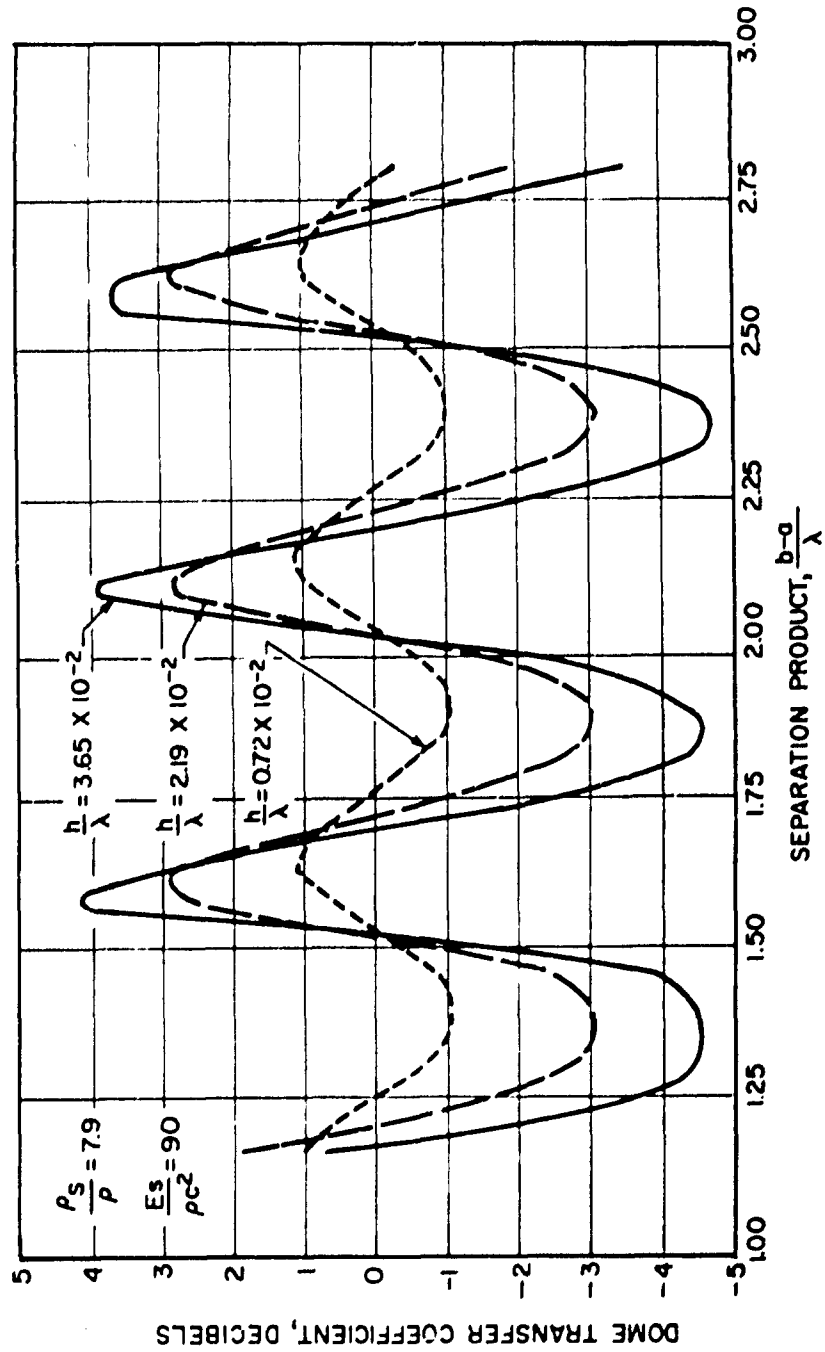AND SEPARATION PRODUCT $\frac{b-a}{\lambda}$

32

IV.   CONCLUSIONS
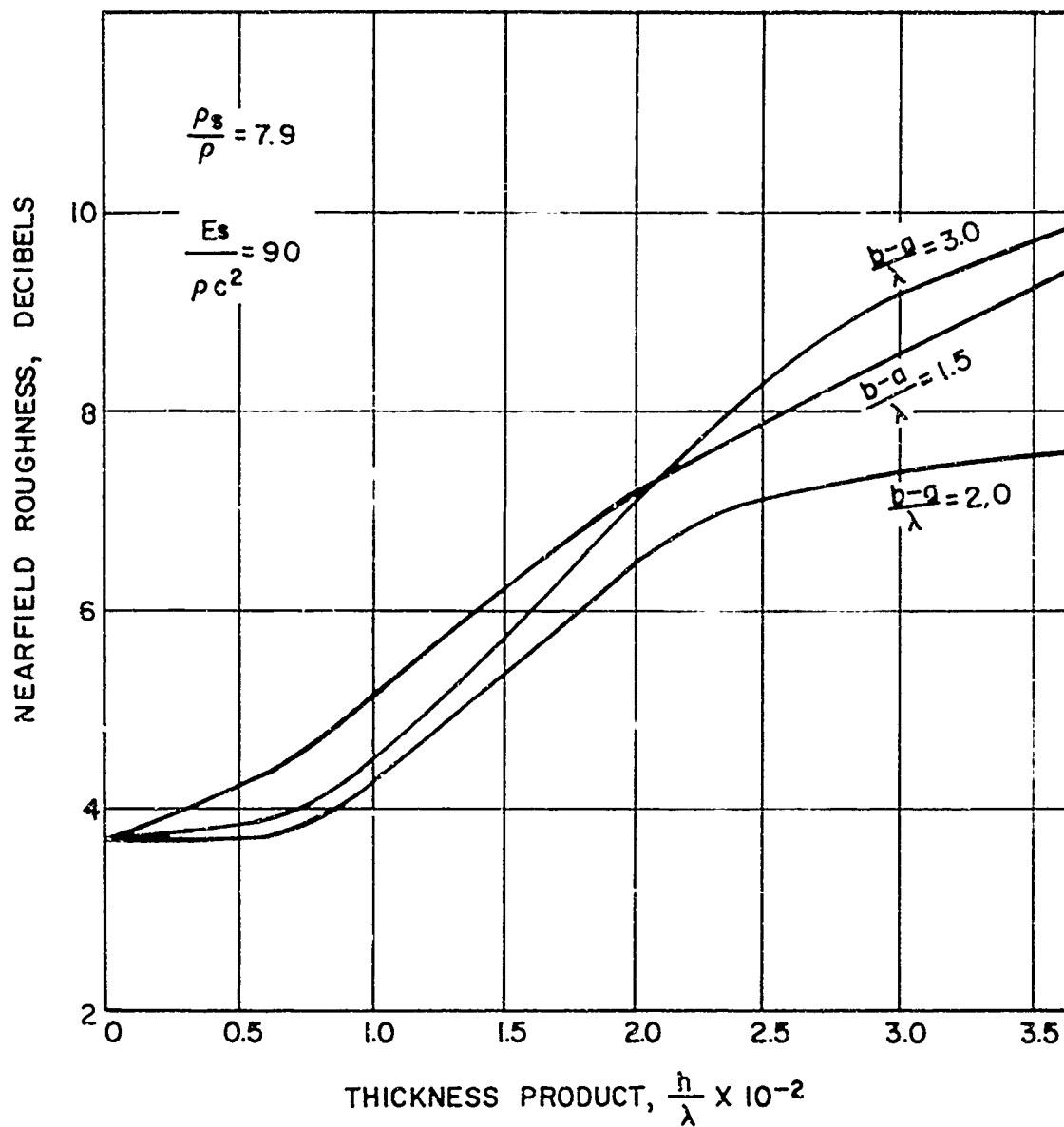
The numerical results presented in this memorandum provide a quantitative measure of the dependence of certain criteria of transducer performance on the geometrical and material parameters of the dome-transducer model. While these results do not apply directly to existing sonar equipments because of the unrealistic dome geometry, some qualitative conclusions can be made in regard to the effects of the sonar dome on system performance.

In general, the dome causes a degradation of all the assumed dome performance criteria, as compared to a transducer without dome. The results indicate that the strongest dependence of the various performance criteria is on the dome thickness product h/λ amd dome density product ρ_s/ρ. Weaker dependence on the dome spacing product $(b-a)/\lambda$ is seen, while the stiffness product $E_s/\rho c^2$ exerts little influence on the performance criteria.

It is helpful in explaining the results to consider the acoustic impedance of the dome. The point acoustic impedance is defined as the ratio of net acoustic pressure to normal particle velocity at the mean surface of the dome. The point impedance Z_n of each mode of the dome is given by[*]

$$Z_n = -i\omega\rho_s h + \frac{ih}{\omega}\frac{E_s}{b^2} + \frac{iE_s h^3}{12\omega b^4}[n^4 - 2n^2 + 1] + \frac{ihn^2 E_s^2}{\omega b^2(\rho_s \omega^2 b^2 - n^2 E_s)} .$$

---

[*]This expression is obtained by solving for the ratio of net acoustic pressure to normal particle velocity in the shell equations describing the motion of the dome. With some manipulation this expression is similar to the result obtained by Heckl[3] and later employed by Barger[4] with the exception that Flugge's shell equations rather than Kennard's have been used in this study. (See Ref. 5.)

From this expression it is obvious that the point impedance is directly proportional to dome density ρ_s and thickness h. Point impedance is inversely proportional to the dome radius b; however, the dependence of Z_n on b is not a strong one. It is seen in the results that each of the performance criteria degrade as Z_n is increased (increasing h/λ or ρ_s/ρ). An increase in $(b-a)/\lambda$ usually leads to a slight improvement in the performance criteria.

Based on these results it appears that the most important dimensionless parameters in the dome-transducer system are the thickness product h/λ and the density product ρ_s/ρ, and that the initial guidelines could be compacted further by computing the dependence of the performance criteria on a new dimensionless variable obtained as the product $h/\lambda \cdot \rho_s/\rho$. From the relation $\lambda = 2\pi c$, where ω is the angular frequency and c is the speed of sound in water, the new dimensionless variable δ can be obtained as $\delta = \dfrac{\omega \rho_s h}{\rho c}$. This expression is seen to be approximately Z_n normalized to the specific impedance of water, or the impedance "mismatch" of the dome.

The results contained in this memorandum support the following specific conclusions regarding the effects of the dome on transducer performance.

1. The performance criteria of the dome-transducer are a strong function of the variable $\omega \rho_s h/\rho c$, an approximate measure of the point impedance of the dome. Improved acoustic performance is obtained by using dome materials having a surface density $\rho_s h$ as small as possible. This conclusion is intuitively obvious for such criteria as Dome Transmission Coefficient, but, more important, is valid for farfield distribution characteristics typified by Directivity Index.

2. Performance criteria are not a strong function of dome-transducer spacing but improve slightly with increased spacing. Variation in power transferred to the water as a result of reflections from the dome are undoubtedly exaggerated by the

34

dome geometry used in this study. However, some interference
can be expected, particularly in domes having broad, near-
concentric windows such as the AN/SQS-26 dome. It should be
noted that scattering from a periodic structure such as a typical
dome supporting structure, not considered in this memorandum,
can complicate further the effects of reflections.

3. Performance criteria are not dependent on the elastic
properties of the dome material. Hence, high-strength materials
should not degrade acoustic performance. It can be concluded
that a low-density, thin dome made of high-strength material
should result in improved acoustic performance and satisfy
strength and durability requirements.

The sets of curves contained in this memorandum are repre-
sentative of the information necessary for the design of sonar
domes on a scientific basis. Improved design guidelines await
the development of more sophisticated analytical models.

V.   REFERENCES

1.   An Improved Analytical Model of the Interaction of Domes and Transducers During Transmission (U), Technical Memorandum, TRACOR Document Number 65-292-U, August 31, 1965.

2.   H. L. Langhaar, Dimensional Analysis and Theory of Models, John Wiley and Sons, New York, 1951.

3.   Manfred Heckl, Vibrations of Point Driven Shells, JASA Cctober, 1962, pp 1553-1557.

4.   J. E. Barger, Sonar Dome Design Guide, Vol. 3, Final Report, Raytheon, NObsr-91145, 1965.

5.   An Analysis of the Interaction of the Sonar Dome and Transducer During Transmission (U), A Summary Report, TRACOR Document Number 65-188-C, May 17, 1965.

TRACOR, INC.   6500 TRACOR LANE, AUSTIN, TEXAS 78721

APPENDIX A

APPENDIX A.   THE SOUND PRESSURE FIELD PRODUCED BY A TRANSDUCER RADIATING IN A CONCENTRIC DOME

The mathematical model illustrated in Figure 1 consists of an infinite-length cylinder and concentric shell. A velocity distribution independent of the axial direction is specified on the surface of the cylinder, and it is desired to find the resulting sound pressure field in the fluid in Regions 1 and 2 of Figure 1. The boundary value problem as stated is a three region problem (two fluid regions and the shell). In general partial differential equations must be solved both in the two fluid regions and in the region of the shell material, and boundary conditions must be matched at shell-fluid interfaces as well as at the cylinder-fluid interface. However, the problem is considerably simplified by using the results of elastic shell theory to describe the motion of the shell's middle surface, thus eliminating the necessity of solving the full partial differential equations of linear elasticity for the shell material. Further, since the shell is thin relative to other geometrical parameters, the boundary conditions at shell-fluid interfaces can be matched at the middle surface of the shell.

A.   Sound Pressure Field in the Fluid

It is assumed that in Regions 1 and 2 the acoustic pressure p obeys the scalar wave equation

$$\frac{1}{r} \frac{\partial}{\partial r} \left(r \frac{\partial p}{\partial r} \right) + \frac{1}{r^2} \frac{\partial^2 p}{\partial \theta^2} = \frac{1}{c^2} \frac{\partial^2 p}{\partial t^2} \tag{1}$$

where r and θ are the space coordinates, t is the time, and c is the propagation velocity in the fluid.

For a harmonic time dependence the general solution to Eq. 1 is
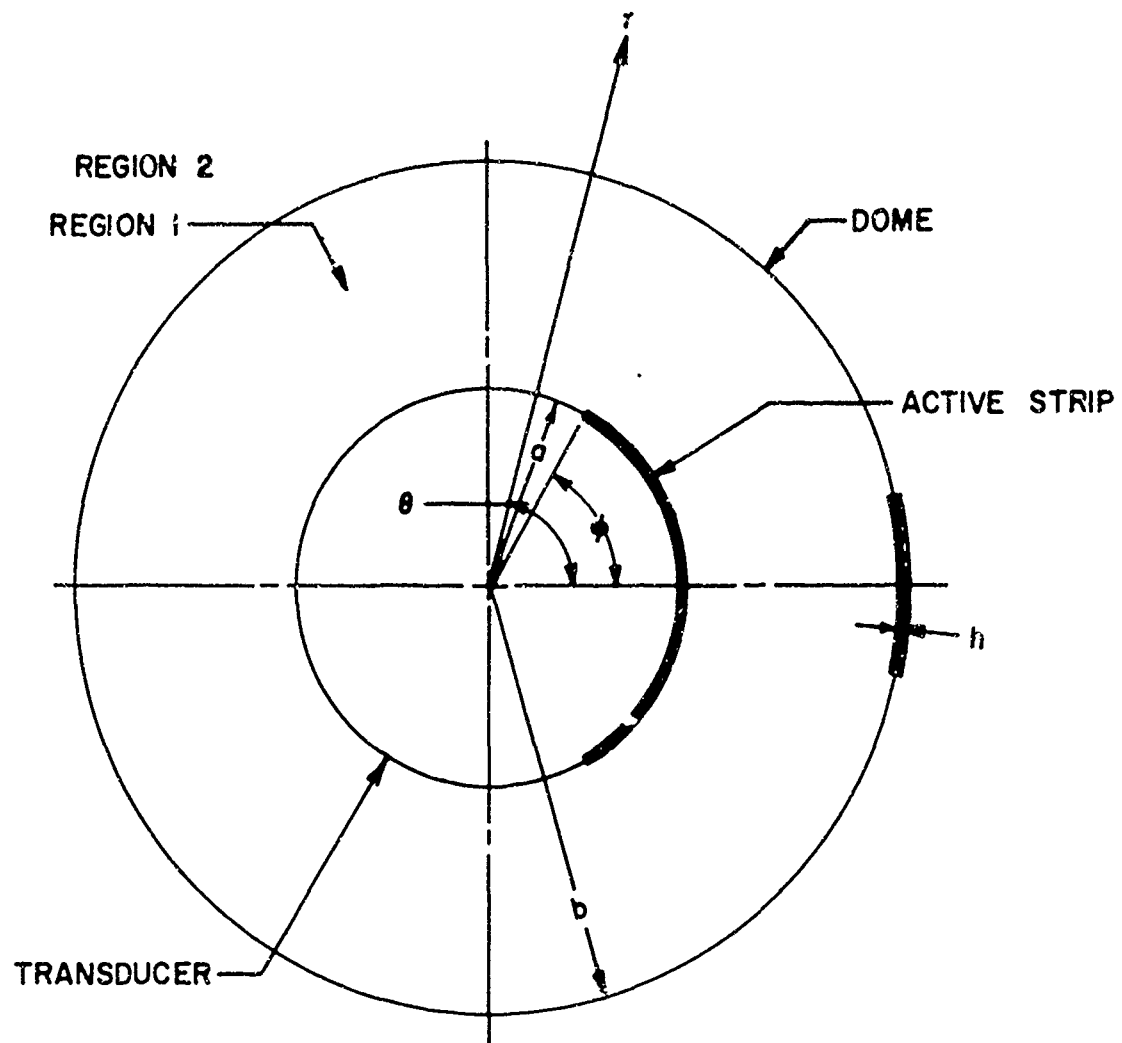
FIG. I – GEOMETRY FOR A CYLINDRICAL TRANSDUCER
RADIATING IN A CONCENTRIC DOME

A-2

$$p = \sum_{n=0}^{\infty} [A_n H_n^{(1)}(kr) + B_n H_n^{(2)}(kr)] \cos n\theta \, e^{-i\omega t} \qquad (2)$$

where $H_n^{(1)}$ and $H_n^{(2)}$ are the nth order Hankel functions of the first and second kind, respectively, ω is the angular frequency, $k = \omega/c$, and A_n and B_n are constants which will be determined by boundary conditions. Equation 2 involves only cosine terms as it is anticipated that problems to be analyzed will possess symmetry about $\theta=0$. In Region 1 the sound pressure field is*

$$P_1 = \sum_{n=0}^{\infty} [A_n H_n^{(1)}(kr) + B_n H_n^{(2)}(kr)] \cos n\theta \quad . \qquad (3)$$

The sound pressure and the radial component v_r of the fluid velocity, with harmonic time dependence, are related by

$$\frac{-1}{\rho} \frac{\partial p}{\partial r} = \frac{\partial v_r}{\partial t} = -i\omega v_r \qquad (4)$$

At the shell-fluid interfaces this component of the fluid velocity must equal the velocity of the shell. (This restriction does not apply to velocity components tangential to the interface because the fluid is regarded as inviscid and hence will not support shear forces.) Denoting the velocity on the cylinder by V_r and the radial component of the velocity of the shell by w, the interface conditions at r=a and r=b are

$$\frac{1}{i\omega\rho} \left. \frac{\partial P_1}{\partial r} \right|_{r=a} = V_r \qquad (5)$$

$$\frac{1}{i\omega\rho} \left. \frac{\partial P_1}{\partial r} \right|_{r=b} = w \quad . \qquad (6)$$

*The time component $e^{-i\omega t}$ will be suppressed in the following.

In the case of interest, a section of the cylinder of angular extent 2φ is phased to represent a plane velocity distribution of uniform amplitude, while the remainder of the cylinder is rigid. This condition can be written as

$$V_r = \frac{1}{\rho c} \cos \theta \; e^{ikacos \; \theta} \quad , \qquad |\theta| < \varphi \quad ,$$

$$= 0 \qquad\qquad , \qquad |\theta| > \varphi \quad . \tag{7}$$

A Fourier series for the function $\cos \theta \; e^{ikrcos \; \theta}$ may be obtained by differentiating the identity,

$$e^{ikrcos \; \theta} = \sum_{n=0}^{\infty} \epsilon_n \; i^n \; J_n(kr) \cos n\theta$$

where $\epsilon_0 = 1$, $\epsilon_n = 2$ for $n > 0$, and J_n is the Bessel function. Then

$$V_r = \frac{1}{i\rho c} \sum_{n=0}^{\infty} \epsilon_n \; i^n \; J_n{}'(ka) \cos n\theta \quad , \quad |\theta| < \varphi \quad ,$$

$$= 0 \qquad\qquad\qquad , \quad |\theta| > \varphi \quad , \tag{8}$$

where the prime indicates a derivative with respect to the argument. Equation 8 can be represented by the Fourier series

$$V_r = \frac{1}{i\rho c} \sum_{n=0}^{\infty} \delta_n \cos n\theta \tag{9}$$

where

$$\delta_n = \epsilon_n \sum_{m=0}^{\infty} \epsilon_m \; i^m \; J_m{}'(ka) \; \begin{Bmatrix} n \\ m \end{Bmatrix}$$

and

A-4

$$\begin{Bmatrix} n \\ m \end{Bmatrix} = \frac{1}{2\pi} \left[\frac{\sin|n+m|\varphi}{|n+m|} + \frac{\sin|n-m|\varphi}{|n-m|} \right] , \quad n \neq m \quad ,$$

$$\begin{Bmatrix} n \\ n \end{Bmatrix} = \frac{1}{2\pi} \left[\frac{\sin 2n\varphi}{2n} + \varphi \right] , \quad n \neq 0 \quad ; \quad \begin{Bmatrix} o \\ o \end{Bmatrix} = \varphi/\pi \quad .$$

The substitution of Equations 2 and 9 into Eq. 5 results in

$$\frac{k}{i\omega\rho} \sum_{n=0}^{\infty} [A_n H_n^{(1)'}(ka) + B_n H_n^{(2)'}(ka)]\cos n\theta = \frac{1}{i\rho c} \sum_{n=0}^{\infty} \delta_n \cos n\theta. \quad (10)$$

Noting that the cosine functions are linearly independent and that $k/\omega = 1/c$, Eq. 10 implies

$$A_n H_n^{(1)'}(ka) + B_n H_n^{(2)'}(ka) = \delta_n \quad . \quad\quad (11)$$

The radial component of the shell velocity can be represented in the form

$$w = \sum_{n=0}^{\infty} G_n \cos n\theta \quad . \quad\quad (12)$$

The boundary condition given by Eq. 6 then becomes

$$\frac{k}{i\omega\rho} \sum_{n=0}^{\infty} [A_n H_n^{(1)'}(kb) + B_n H_n^{(2)'}(kb)]\cos n\theta = \sum_{n=0}^{\infty} G_n \cos n\theta \quad (13)$$

or

$$A_n H_n^{(1)'}(kb) + B_n H_n^{(2)'}(kb) = ic\rho G_n \quad\quad (14)$$

since the cosine functions are linearly independent.

A-5

In writing the general solution for the sound pressure p_2 outside the shell it is necessary to account for the fact that, for large r, the pressure field should have the form of an outgoing wave. Since

$$\lim_{r \to \infty} \left\{ e^{-i\omega t} H_n^{(1)}(kr) \right\} = e^{i(kr - \omega t)} \sqrt{2/\pi \, kr}$$

represents an outgoing wave, the proper form for p_2 is

$$p_2 = \sum_{n=0}^{\infty} C_n H_n^{(1)}(kr) \cos n\theta \quad . \tag{15}$$

The interface condition on the velocities of the fluid and shell on the outside surface of the shell will be matched at the middle surface of the shell, as in Eq. 6. Hence

$$\frac{1}{i\omega\rho} \left. \frac{\partial p_2}{\partial r} \right|_{r=b} = w$$

or

$$\frac{k}{i\omega\rho} \sum_{n=0}^{\infty} C_n H_n^{(1)\prime}(kb) \cos n\theta = \sum_{n=0}^{\infty} G_n \cos n\theta, \tag{16}$$

and, noting the linear independence of the cosine functions,

$$C_n H_n^{(1)\prime}(kb) = ic\rho \, G_n \quad . \tag{17}$$

Equations 11, 14, and 17 give three sets conditions on the four sets of unknowns, A_n, B_n, C_n, and G_n. A consideration of the motion of the shell is necessary to obtain the requisite fourth condition.

B. <u>Motion of the Shell</u>

Let the radial and tangential displacements from
equilibrium of the middle surface of the shell be denoted by
u_r and u_θ, respectively. Flügge's shell equations are

$$\rho_s \frac{\partial^2 u_\theta}{\partial t^2} = \frac{E_s}{b^2} [\frac{\partial^2 u_\theta}{\partial \theta^2} + \frac{\partial u_r}{\partial \theta}] \qquad (18)$$

$$\rho_s \frac{\partial^2 u_r}{\partial t^2} = \frac{p_- - p_+}{h} - \frac{E_s}{b^2} [\frac{\partial u_\theta}{\partial \theta} + u_r] - \frac{E_s h^2}{12 b^4} [\frac{\partial^4 u_r}{\partial \theta^4} + 2 \frac{\partial^2 u_r}{\partial \theta^2} + u_r] \quad (19)$$

where h is the thickness of the shell and b is the radius of its
middle surface, ρ_s is the mass density of the shell material and
$E_s = E/(1-\nu^2)$, E being Young's modulus and ν Poisson's ratio.
p_- and p_+ are the pressures on the inside and outside shell
surfaces, respectively, so $p_- = [p_1]_{r=b}$ and $p_+ = [p_2]_{r=b}$.
Since w is the radial velocity of the shell,

$$w = \frac{\partial u_r}{\partial t} = -i\omega u_r . \qquad (20)$$

The tangential velocity v of a shell element is represented as

$$v = \frac{\partial u_\theta}{\partial t} = -i\omega u_\theta \qquad (21)$$

For symmetry about $\theta=0$, the Fourier series representation for v
is of the form

$$v = \sum_{n=0}^{\infty} D_n \, \text{Sin} \, n\theta . \qquad (22)$$

The shell Equations 18 and 19 can be differentiated with
respect to time to give conditions on u and v.

$$-\omega^2 \rho_s v = \frac{E_s}{b^2} [\frac{\partial^2 v}{\partial \theta^2} + \frac{\partial w}{\partial \theta}] \tag{23}$$

$$-\omega^2 \rho_s w = -\frac{i\omega}{h} [P_1|_{r=b} - P_2|_{r=b}] - \frac{E_s}{b^2} [\frac{\partial v}{\partial \theta} + w]$$

$$- \frac{E_s}{12b^4} [\frac{\partial^4 w}{\partial \theta^4} + 2 \frac{\partial^2 w}{\partial \theta^2} + w] \ . \tag{24}$$

If Equations 4, 16 and the Fourier series for w and v are substituted into Equations 23 and 24 and the linear independence of the trigonometric functions employed, the following conditions are obtained.

$$-i\omega [H_n^{(1)}(kb) A_n + H_n^{(2)}(kb) B_n] + i\omega H_n^{(1)}(kb) C_n - \frac{h E_s n}{b^2} D_n$$

$$+ h \left\{ \omega^2 \rho_s - \frac{E_s}{b^2} [1 + \frac{h^2}{12b^2}(n^4 - 2n^2 + 1)] \right\} G_n = 0 \tag{25}$$

$$\left\{ \omega^2 \rho_s - \frac{E_s}{b^2} n^2 \right\} D_n - \frac{E_s}{b^2} n G_n = 0 \quad . \tag{26}$$

C.   Determination of the Coefficients

Equations 13, 15, 18, 25, and 26 represent a set of simultaneous algebraic equations in the unknowns A_n, B_n, C_n, D_n, and G_n. This set of equations is readily solved to complete the solutions for the sound pressure field in Regions 1 and 2 given by Equations 3 and 15 respectively.

As an example of the form of the coefficients, the solution for the set of coefficients C_n which are associated with p_2 (Eq. 15) is

$$C_n = \frac{\delta_n}{H_n^{1}{}'(ka) + h \gamma_n H_n^{1}{}'(kb) [J_n'(kb) N_n'(ka) - N_n'(kb) J_n'(ka)]} \quad (27)$$

where

$$\gamma_n = \frac{\pi b}{2c^2 \rho} \left\{ \omega^2 \rho_s - \frac{E_s}{b^2} [1 + \frac{h^2}{12b^2} (n^4 - 2n^2 + 1)] - \frac{E_s^2 n^2}{b^2(b^2\omega^2\rho_s - E_s n^2)} \right\} .$$

This form is typical of the remaining coefficients. It is of interest to note that for h = 0, the C_n reduce to the coefficients obtained for a transducer radiating without a dome.

APPENDIX B. DETERMINATION OF TRANSMISSION COEFFICIENT

It is often helpful to relate certain phenomena associated
with sound transmission through shells to their analogues in the
theory of plane wave transmission through plates. In the latter
area of study there are basically two types of problems, one
in which the velocity distribution is specified on the surface
radiating the pressure wave and the other in which the form of
the plane wave incident on the plate is specified. Of course,
the first type of problem more nearly approximates reality in
that it takes into account coupling between the plate and the
radiating surface (multiple reflections, etc.). But the second
type of problem is particularly well suited for studying proper-
ties of the plate itself and is usually the problem seen in the
literature.

In the second type of problem, the form of the incident
wave is given and the waves transmitted through and reflected
from the plate are calculated. Then a plate transmission co-
efficient T can be defined as the ratio of the amplitude of the
transmitted wave to the amplitude of the incident wave. If the
incident wave is not a plane wave but is a type of wave which
would be emitted by a finite source, the transmission coefficient
can be defined as the ratio of power transmitted through the
plate to power incident on the plate. In this case the trans-
mission coefficient is a function of the form, but not of the
amplitude, of the incident wave. For a given form of incident
wave the transmission coefficient depends only on plate parameters.

The basic problem described in Ref. 1 is analogous to the
first type of plane wave problem mentioned above in that the
coupling between the cylindrical shell and the cylindrical radi-
ating surface transducer is included. However, in this problem
it is impossible to separate the resultant field between the
transducer and shell into incident and reflected parts and thus
define a transmission coefficient. Nevertheless, it is possible

to formulate a problem analogous to the second type of plane wave problem mentioned above by specifying the form of the incident cylindrical wave and calculating the transmitted wave. Then a transmission coefficient can be defined as the ratio of power transmitted through the shell to power incident on the shell. Of course, in this type of problem the wave reflected inward from the shell is not scattered back toward the shell; that is, multiple reflections are not included. The transmission coefficient will be a function of the form of the incident wave; however, it should not vary much among those types of waveforms which represent directed beams.

A typical directed beam is that produced by a cylindrical transducer driven in the manner described in detail in Ref. 1. To obtain this beam the elements on a 120° section of the cylinder surface are driven with the phase and amplitude distribution of a plane wave. The amplitude and phase of the jth element will be denoted by S_j and ω_j, respectively, and the driving and response will be assumed to have an $e^{-i\omega t}$ time dependence. Then the velocity of the fluid at the surface of the transducer can be expanded in a Fourier series in the θ coordinate of the cylindrical coordinate system r, θ, the surface of the transducer being $r = a$. Thus

$$v = \frac{e^{-i\omega t}}{i\omega\rho} \sum_{n=o}^{\infty} \delta_n \cos n\theta \quad , \tag{1}$$

where ρ is the fluid density and

$$\delta_n = i\omega\rho \frac{2}{n\pi} \sum_{j=o}^{\infty} S_j e^{i\omega j} \left[\sin n[(2j-1)\alpha+\beta] - \sin n[(2j-1)\alpha-\beta] \right] \quad , \tag{2}$$

with 2β the angular width of the elements and 2β their angular spacing. The resulting directed beam is then p_{inc},

$$p_{inc} = e^{-i\omega t} \sum_{n=0}^{\infty} A_n H_n^{(1)}(kr) \cos n\theta \quad , \tag{3}$$

where $H_n^{(1)}(kr)$ is a Hankel function of the first kind, k is the ratio of ω to the speed of sound c in the fluid, and

$$A_n = \delta_n / H_n^{(1)\prime}(ka) \quad , \tag{4}$$

the prime denoting differentiation with respect to argument.

In order to calculate a transmission coefficient for the shell it will be assumed that the pressure wave, Eq. (3), can be generated within the shell and directed at the shell surface so that the radiated energy will be partly transmitted through the shell and partly reflected. The transmitted and reflected pressure fields, p_t and p_r, respectively, have the forms

$$p_t = e^{-i\omega t} \sum_{n=0}^{\infty} C_n H_n^{(1)}(kr) \cos n\theta \quad , \tag{5}$$

$$p_r = e^{-i\omega t} \sum_{n=0}^{\infty} B_n H_n^{(2)}(kr) \cos n\theta \quad , \tag{6}$$

where $H_n^{(2)}(kr)$ is a Hankel function of the second kind, and B_n and C_n are constants which will be determined by conditions at the shell, at r = b. It should be noted that, for an $e^{-i\omega t}$ time dependence, the $H^{(1)}$ Hankel functions represent outgoing waves and the $H^{(2)}$ Hankel functions represent ingoing waves. The pressure field inside the shell is the sum $p_{inc} + p_r$.

B3

The method of analysis proceeds exactly as in Ref. 1.
The pressure fields are substituted into shell equations involving the shell velocity components, Fourier series are ass' ned for these velocity components, then the coefficients 'n these series and in the series of Eqs. (5) and (6) can be determined.

$$B_n = \frac{i\ D_n\ A_n}{1 - i\ D_n} \tag{7}$$

$$C_n = \frac{A_n}{1 - i\ D_n} \tag{8}$$

In these expressions

$$D_n = \frac{\pi bh}{4c^2 \rho}\ |H_n^{(1)\,\prime}(kb)|^2\ \left\{ \omega^2 \rho_s - \frac{E_s}{b^2}\ [1 + \frac{h^2}{12b^2}(n^2-1)^2] - \frac{E_s^2\ n^2}{b^2[b^2\omega^2 \rho_s - E_s n^2]} \right\}$$

h is the shell thickness, ρ_s its mass density and $E_s = E/(1-\nu^2)$, where E is Young's modulus and ν is Poisson's ratio. The pressure fields are completely determined.

The average power inc ident on the shell and transmitted through the shell are then

$$\text{Power Incident} = \frac{2}{\omega \rho}\ \sum_{n=o}^{\infty} \frac{1}{\epsilon_n}\ |A_n|^2 \tag{9}$$

$$\text{Power Transmitted} = \frac{2}{\omega \rho}\ \sum_{n=o}^{\infty} \frac{1}{\epsilon_n}\ |C_n|^2\ , \tag{10}$$

where $\epsilon_o = 1$, $\epsilon_n = 2$ for $n > 1$. The transmission coefficient T is defined as

$$T = \frac{\text{Power Transmitted}}{\text{Power Incident}} \tag{11}$$

END

DATE
FILMED

3-11-66